POLITECNICO DI TORINO

Master's Degree in Course Aerospace Engineering

Master's Degree Thesis

Mission Analysis of a CubeSat for Hyperspectral Remote Sensing in Low Earth Orbit

Supervisors

Prof.ssa Manuela BATTIPEDE

Ing. Luigi MASCOLO

Co-Supervisor

Ing. Valerio GIULIANI

Candidate

Mario PAGGIARINO

Academic Year 2020/2021

Summary

The purpose of this work is to perform a feasibility study of a mission involving the analysis of the biodiversity of terrestrial areas in collaboration with S.A.B Aerospace of Benevento, using a Cubesat platform and commercial Off-the-Shelf component.

The orbit choice, by the mission prerequisites, was evaluated taking into account the performance of the Hyperspectral camera mounted on board and its specifications, so that the satellite would be able to acquire sufficient data during the passage over the areas of interest.

Finally, by calculating the data rate generated by the payload and the telemetry and command data, a link budget was evaluated to guarantee correct and efficient communication with the ground stations of LeafSpace network involved.

Ringraziamenti

Giunto al termine di questo percorso, segnato da non poche difficoltà ed imprevisti, ci tengo a ringraziare la S.A.B Aerospace per avermi concesso la possibilità di lavorare a questo progetto ed in particolare il mio tutor Ing. Valerio Giuliani che, grazie alla sua disponibilità e la sua esperienza è sempre stato capace di fornirmi il suggerimento giusto per proseguire con il lavoro.

Una menzione speciale va alla mia relatrice, la professoressa Manuela Battipede e al correlatore Ing. Luigi Mascolo, la cui passione e dedizione verso gli argomenti trattati a lezione, è stata per me stimolo e fonte di ispirazione. Un sincero ringraziamento per la disponibilità e la gentilezza dimostratami e per avermi concesso l'occasione di lavorare con loro.

Table of Contents

List of Tables

List of Figures

Acronyms

BPSK
: Binary phase-shift keying

CAGR
: Compound Annual Growth Rate

COTS
: Commercial off-the-shelf components

ECEF
: Earth-centered coordinate system

FOV
: Field of View

FSK
: Frequency shift keying

HSI
: Hyperspectral Imaging System

LTDN
: Local Time of Descending Node

MSI
: Multispectral Imaging System

OBC
: Onboard Computer

RF

Radio Frequency

RS

Remote Sensing

STK

System Tool Kit

UAS

Unmanned aerial systems

Chapter 1

Introduction

Access to space has always required numerous investments in terms of cost and time. What in the past was seen as an accessible sector for institutional entities, today, with technological progress that guarantees an affordable investment for private individuals, has given a cultural revolution in what can be defined as the New Space Economy. The economic returns behind these investments lead to greater competitiveness among companies and increasingly flourishing development of the space industry.

As a part of this revolution, it is possible to identify the development of CubeSat, cubical-shaped small satellite , born to reduce costs and development time, to increase accessibility to space, and support more frequent launches.

1.1 CubeSat Background

The CubeSat project began in 1999 as a collaboration between Professor Bob Twiggs at Stanford University's Space Systems Development Laboratory (SSDL) and Professor Jordi PuigSuari at California Polytechnic State University (Cal Poly), San Luis Obispo [1]. The purpose was to create a standard for small satellites affordable for everyone, including college students, with low design and manufacturing costs.

A CubeSat has a size of 10 cm per side and weights up to 1.33 kg. It is the basic unit for these satellites, '1U', which are modular to achieve CubeSat of different sizes '2U', '3U', '6U', '12U', according to mission requirements. The small size allows the launch in piggyback with primary satellites, using the extra space available in the launcher, and ensures the possibility of building constellations of multiple satellites deployable in a single launch, thus lowering the launch cost.

The CubeSat market is growing due to its flexibility in performing different types of missions, like developing and demonstrating the technology, telecommunications, Earth observations, and monitoring of environmental phenomena. Their success is also due to the miniaturization of electronic components and related subsystems, which have given them capabilities similar to those of larger satellites, leading to an ever-growing market of commercial off-the-shelf components (COTS), available even by private customers.

According to Allied Market Research's market forecast [2], the global CubeSat industry raised $210.1 million in 2019 and is expected to reach $491.3 million by 2027, with a compound annual growth rate (CAGR) of 15.1% from 2020 to 2027. As shown in [fig 1.1] the CubeSat business increases beyond any statistical predictions, as evidenced by the data above.

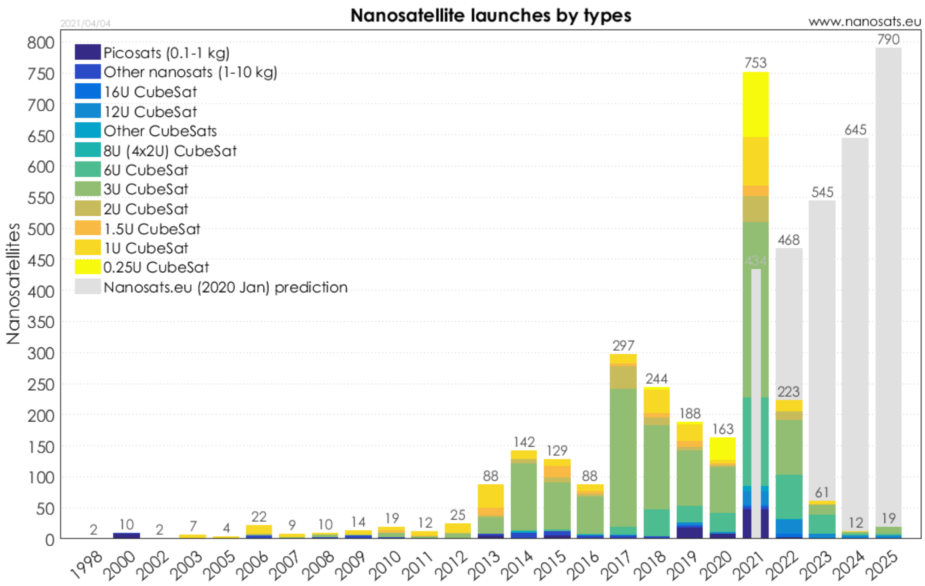

Figure 1.1: Launched, planned and predicted CubeSats as of January 2020 [3].

Based on application, Earth monitoring and observation missions accounted for the largest share of the global CubeSat market in 2019 and are estimated to continue to hold this status over the years, given the economic benefits and rapid development cycles. These types of missions are increasingly being joined by technology ones, given the numerous investments in science experiments and research, which are expected to achieve the highest compound annual growth rate between 2020 and 2027, peaking at 16%.

Based on end-user, the commercial segment contributed the largest market share, accounting for more than half of the global CubeSat market in 2019, and will maintain its leading position during the forecast period. Moreover, this segment is estimated to witness the fastest CAGR of 15.6% from 2020 to 2027. It is attributed to the increasing demand for obtaining high-resolution terrestrial imaging and communication services.

1.2 Remote Sensing

Remote sensing is the science of getting information by observing a medium, a process, a phenomenon without ever coming into direct contact with that phenomenon, actually providing a different perspective on things.

According to the most generally accepted meaning refers to techniques based on instruments used in the acquisition and measurement of data and information as shown in [fig 1.2]

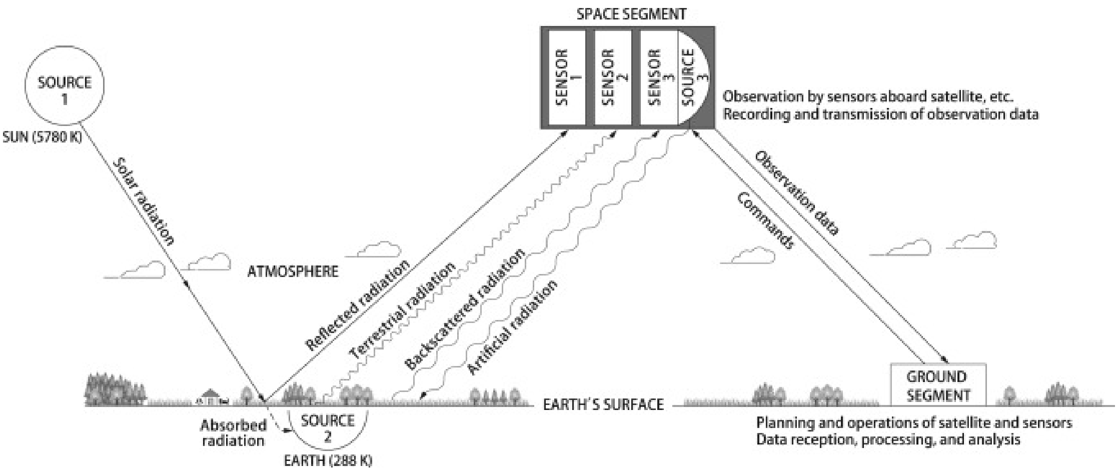

Figure 1.2: Remote Sensing from satellite [4].

The official entry of sensors into space began with the addition of an automatic camera aboard German V-2 rockets launched from the White Sands, NM. The advent of Sputnik in 1957 made it possible to mount cameras on orbiting spacecraft. The first cosmonauts and astronauts documented the circumnavigation of the globe by shooting from space. Sensors capturing black and white images of the Earth were mounted on meteorological satellites starting in 1960.

Remote sensing reached a later maturity, with operational systems for the acquisition of images of the Earth with a certain periodicity, in 1970 with instruments aboard Skylab (and later the Space Shuttle) and on Landsat, the first satellite expressly dedicated to the monitoring of land and oceans to map cultural and natural resources [5].

Remote sensing instruments are of two primary types: passive and active sensors. The first ones can detect information, in the case of the visible spectrum, only due to sunlight reflected from the target, limiting their use depending on lighting conditions.

Active sensors acting as energy sensors illuminate the target reflecting this radiation, detected and measured by the satellite, thus operating in any lighting condition. As for the thermal infrared instead, it can be recorded in any lighting condition, provided that the amount of energy is large enough to be detected.

Remote sensing images are generated based on three different types of resolution:

1. Spatial Resolution

2. Radiometric Resolution

3. Spectral Resolution

Spatial resolution refers to the size of the lowest possible feature that capable of being detected. For satellite observations, spatial resolution is denoted in the coarseness or fineness of a raster grid, where each cell corresponds to an area of observed terrain. The higher the spatial resolution of a digital image, the more details it contains [fig 1.3] and is fundamental in some applications, although expensive due to the large number of data to be stored.

Figure 1.3: Example of higher (left) to lower (right) spatial resolution representing the same land [6].

Although data compression techniques significantly reduce storage requirements, the storage and processing costs associated with high-resolution satellite data often make medium and low-resolution data preferable for large-area analysis.

Radiometric resolution refers to a sensor's ability to discriminate slight differences in the magnitude of radiation within the terrain area that corresponds to a single raster cell.The radiometric resolution is expressed as several bits, typically in the range of 8 to 16 bits. These bits represent the number of different intensities of radiation that the sensor can distinguish and record. The greater the bit depth (number of data bits per pixel) of the images a sensor records, the greater its radiometric resolution.

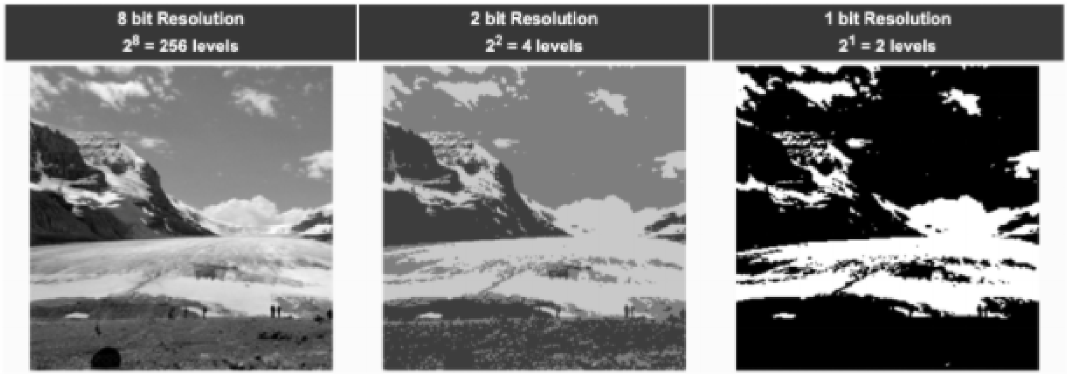

Figure 1.4: From left to right, 8 bit, 2 bit and 1 bit radiometric resolutions are shown [7].

Spectral resolution is the ability of a sensor to detect narrow differences in wavelength, in short, the number and size of bands in the electromagnetic spectrum that the sensor can capture. Low-resolution sensors record energy within relatively broad wavelength bands, while high-resolution sensors record energy within narrow bands [fig 1.6].

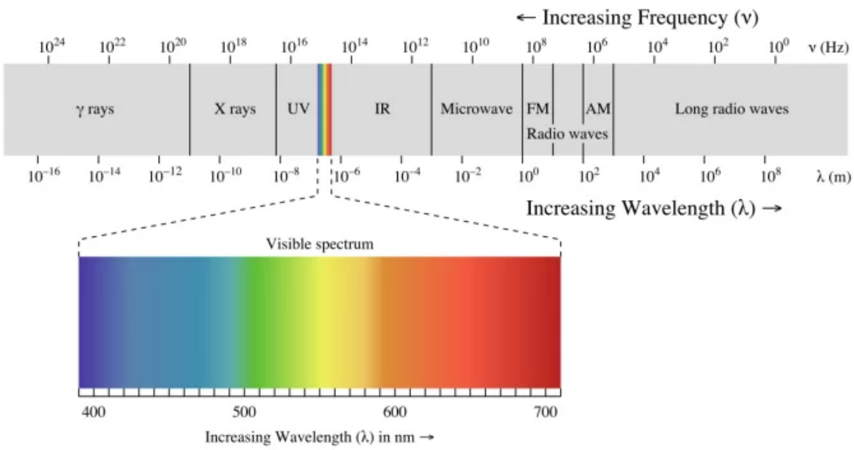

Figure 1.5: The electromagnetic spectrum of light.

Remote sensing data represents a snapshot in time. Temporal resolution refers to the ability of satellites to provide images of the same geographic area more frequently, also known as "return time" or "revisit time". The temporal resolution depends primarily on the platform, e.g., satellites usually have established return times while sensors mounted on aircraft or Unmanned aerial systems (UAS) typically show variable return times. For satellites, the return time depends on orbital characteristics (low or high orbit), strip width, and whether or not the sensor can be pointed in a desired direction.

Satellite observations allow better assessment of spectral, spatial, and physical properties, making field sampling more targeted, efficient, and reliable by covering large areas over inaccessible regions. They provide detailed information on target characteristics at regional or global scales, with variable spectral responses and different time scales [8].

1.3 Hyperspectral Imaging

Hyperspectral sensors (HSI) have a very high spectral resolution, thus collecting several spectral bands from the visible, near-infrared, mid-infrared, and shortwave infrared portions of the electromagnetic spectrum enabling the construction of a near-continuous spectral reflectance signature.

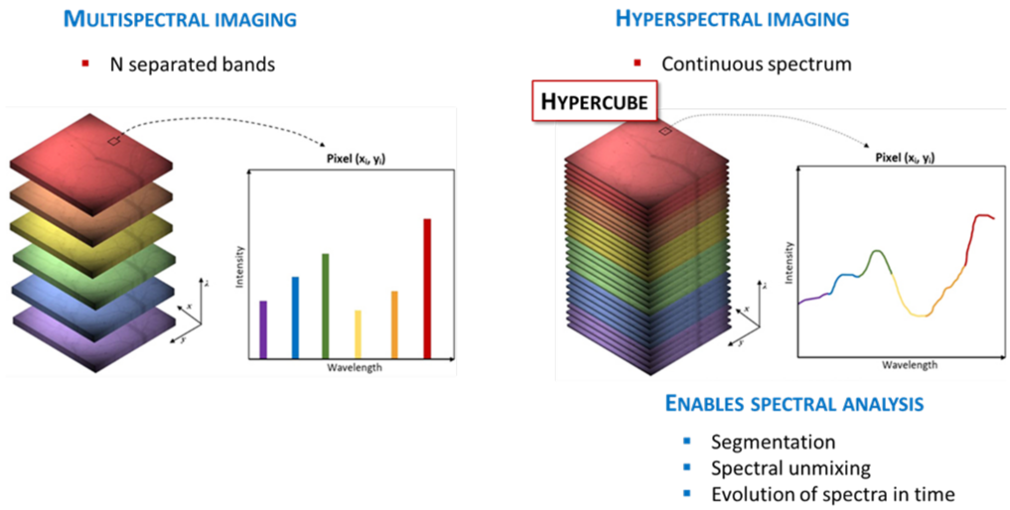

Figure 1.6: Spectral bands comparison between multispectral imaging (left) and hyperspectral imaging (right)

In addition, the narrow bandwidths characteristic of hyperspectral data allow for an in-depth examination of features of the Earth's surface that would otherwise be lost in the relatively coarse bandwidths obtained through multispectral sensors, which unlike the effectively continuous wavelength data collection of a hyperspectral imaging system (HSI), a multispectral imaging system (MSI) focuses on several preselected wavebands based on the application at hand [fig 1.6].

Data acquisition methods can be divided into four main categories [9]:

1. The whiskbroom scanning - a process that acquires spectral information for one spatial coordinate at a time. This method offers the highest level of spectral resolution but requires the system to scan the target area on both the x and y axes.

2. The push-broom scanning - a linear scan data acquisition in which a single axis of spatial motion is required as a row of pixels scrolls over an area to capture spectral and positional information. These push-broom systems can have compact size, reduced weight, simpler operation, and a higher signal-to-noise ratio.

3. The plane scanning - photograph of the entire 2D area at once, but at each wavelength interval and involves numerous image acquisitions to create the spectral depth of the hyperspectral data cube.This acquisition method does not require translation of the sensor or the complete system, but the subject should not move during acquisition to avoid compromising the accuracy of the positional and spectral information.

4. Single shot or snapshot scanning - that collects the entire cube of hyperspectral data in a single integration period. Although single-shot appears to be the preferred future of HSI implementation, it is now limited by a relatively lower spatial resolution.

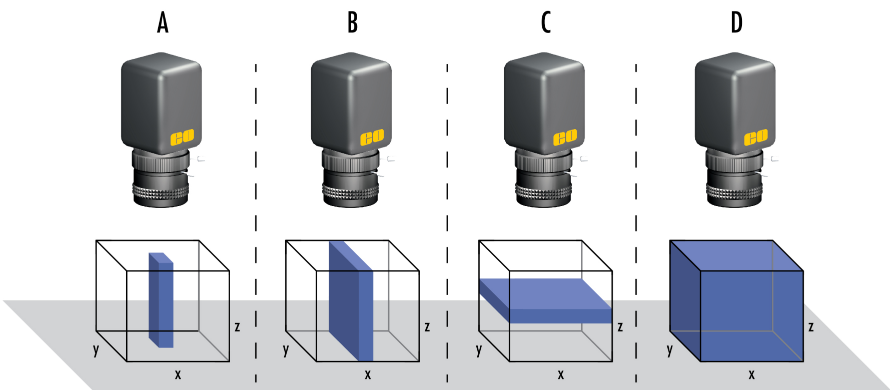

Figure 1.7: Different scanning methods for acquisition data. [9]

The pre-processing phase of hyperspectral data is usually followed by a size reduction operation that handles hyperspectral data to more efficiently address dimensionality issues that harm computational processing in general.[10]

This technology is increasingly trending in several areas and will continue to grow despite slow industry adoption. Spectral photography can penetrate through the Earth's atmosphere and various cloud covers for an unobscured view of the underlying terrain. Thus, it can be used to monitor population changes, observe geological transformations, and study archaeological sites.

In addition, HSI and MSI technologies have become increasingly critical in the study of the environment. It is possible to collect data on deforestation, ecosystem degradation, carbon recycling, and increasingly erratic weather patterns.[9]

Chapter 2

Orbital Mechanics

The study of the motion of celestial bodies and, similarly, of the orbit trajectory of a satellite, under the action of mutual gravitational attraction, is based on the hypothesis that the bodies themselves are considered a set of material points.

Based on these conditions, the n-body problem is defined, then the conditions under which this model is referable to the two-body problem are evaluated. In this regard, we use the three laws of Kepler to verify how, under certain conditions, the polar equation of trajectory coincides with a polar equation of a conic.

Between 1609 and 1619, due to the study of observation data obtained by the Danish Tycho Brahe, Johannes Kepler formulated the three laws that describe the motion of celestial bodies:

1. The orbit of each planet is an ellipse, with the Sun at one focus.

2. The line joining the planet to the Sun sweeps out equal areas in equal times.

3. The square of the period of a planet is proportional to the cube of its mean distance from the Sun.

Even today, these laws provide a reliable model to describe the motion related to celestial bodies.

2.1 Reference Systems

The study of the motion of orbiting bodies, depending on the mission, requires the introduction of reference systems. Starting from a case as generic as possible it can be considered the *heliocentric reference system* with a fundamental plane based on the ecliptic, whose origin coincides with the center of mass of the Sun.

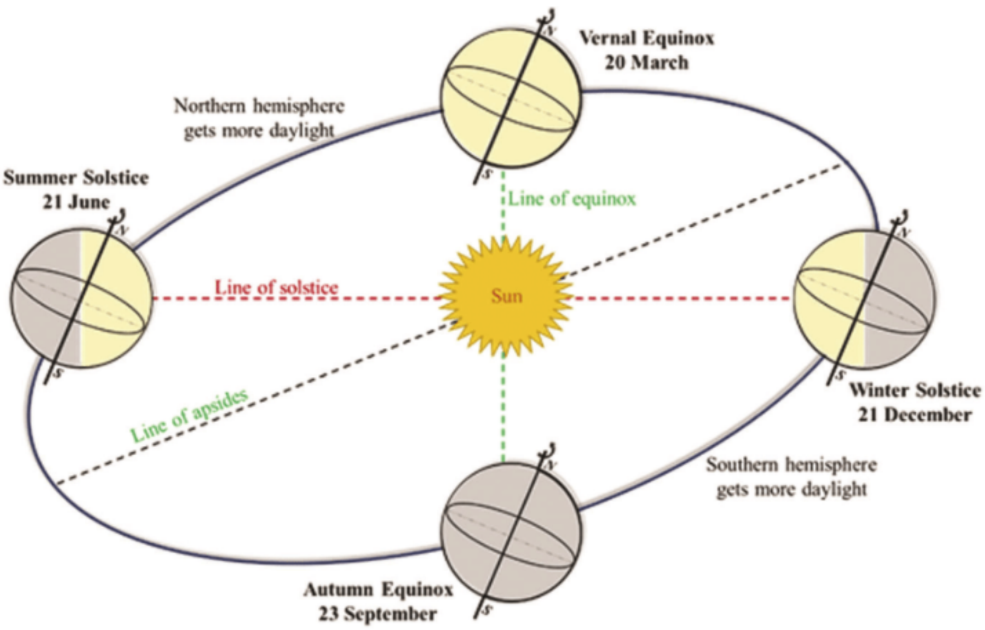

Figure 2.1: Heliocentric-ecliptic reference system

Consider the intersection of the ecliptic plane and the equatorial plane that identifies the direction of the x-axis. At the vernal equinox, the line between the center of the Earth and the center of the Sun points in the positive direction of the x-axis (Υ). The z-axis has positive direction in the direction of the hemisphere that contains Polaris, while the y-axis is identified by the orthogonality of the previous two.

Due to some perturbative actions that result in a slow-motion of the Earth's axis, such a system is not perfectly inertial. In this regard, there is a precession of the ecliptic plane due to the gravitational attraction of the planets, or a precession of the Earth's rotation axis due to the non-sphericity of the Earth and finally a nutation phenomenon due to the torque exerted by the Moon on the Earth's axis, which determines a periodic oscillation.[11]

Then introduce the *Geocentric-Equatorial reference system* with the equator as a fundamental plane, the x-axis pointing in the direction of Υ and the z-axis pointing in the direction of the Earth's North Pole, finally the y-axis once again is obtained by the orthogonality of the two.

It is a non-inertial system due to the motion of the Earth's revolution around the Sun and not integral to the Earth since it does not follow the rotation around the z-axis. Generally, the versors are indicated with $\mathbf{i}, \mathbf{j}, \mathbf{k}$ and for this reason, it is often indicated with the acronym IJK.

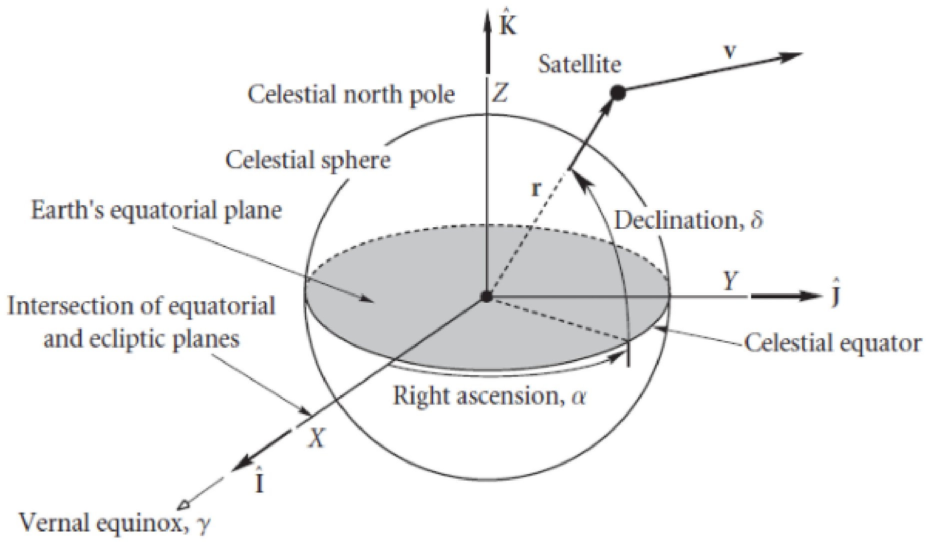

Figure 2.2: Geocentric-Equatorial reference system

The parameters that identify the position of a body can then be expressed in different ways, considering for example the Cartesian coordinates (x, y, z) or according to the right ascension, declination, and distance from the center of the Earth (α, δ, r) and finally by longitude, latitude, and geodetic height of the object (λ, ϕ, h).

Finally, also given the analysis of orbital perturbations, it is possible to consider the RTN *reference system* whose origin coincides with the center of mass of the satellite and has versors $\mathbf{i}_R, \mathbf{i}_T, \mathbf{i}_N$. The versor $\mathbf{i}_R$ is directed along the local radial and points outward from the attractor body, $\mathbf{i}_T$ lies in the plane of instantaneous motion and is concordant with the velocity vector, and $\mathbf{i}_N$ is perpendicular to the $(\mathbf{r}, \mathbf{v})$ plane and concordant with the angular momentum $\mathbf{h}$.[11]

2.2 N-body Problem

The problem of N bodies consists in the study of the relative motion of a system of bodies assimilated to N material points $P_1, ..., P_N$ of masses $m_1, ..., m_N$ respectively, subject to mutual gravitational interactions described by Newtonian law. In particular, introducing the inertial reference system T (O; x, y, z), the motion of the material point m_i, subject to the gravitational action of the other $n-1$ masses and other non-gravitational forces, will be analyzed.[11] It is possible to express

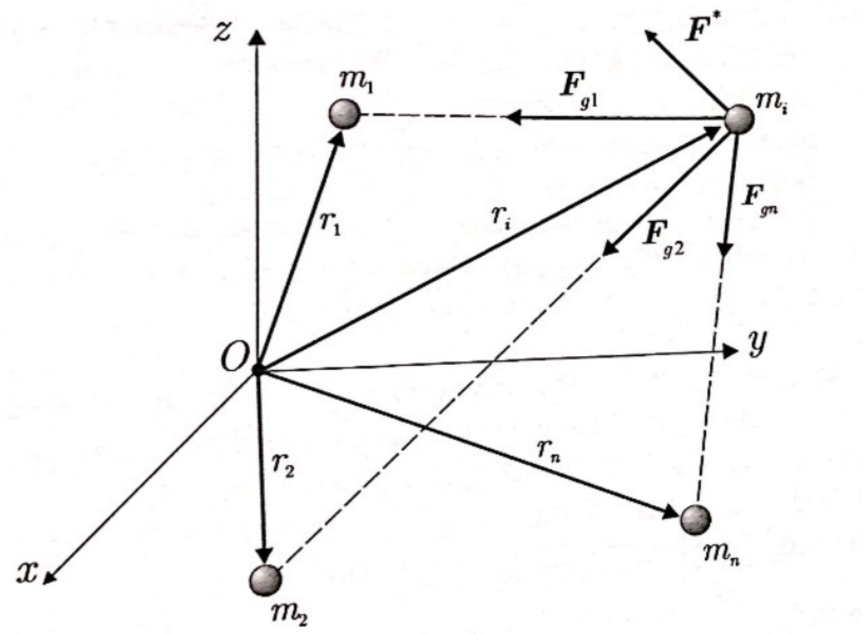

Figure 2.3: Forces acting on the mass m_i of the n-bodies system

the summation of these forces acting on i-th body as follows:

$$\mathbf{F} = \mathbf{F}_{ng} + \sum_{\substack{j=1 \\ j \neq i}}^{n} \mathbf{F}_{gj} \tag{2.1}$$

where $\mathbf{F}_{ng}$ is the results of the aerodynamic forces, solar radiation pressure, propulsive thrust, etc., while $\mathbf{F}_{gj}$ represents the gravitational force due to the j-th body. Given $\mathbf{r}_j$ the position vector linking the j-th body with the origin of the reference system, the i body undergoes an attraction force due to the j body given by:

$$\mathbf{F}_{gj} = -G\frac{m_i m_j}{r_{ij}^3}\mathbf{r}_{ji} \tag{2.2}$$

where $\mathbf{r}_{ji}$ is the position vector connecting body j with body i and G is the universal gravitational constant. It is possible to rewrite everything as follows:

$$\mathbf{F} = \mathbf{F}_{ng} - Gm_i \sum_{\substack{j=1 \\ j \neq i}}^{n} \frac{m_j}{r_{ij}^3}\mathbf{r}_i j \tag{2.3}$$

where:

$$\mathbf{r}_{ji} = \mathbf{r}_i - \mathbf{r}_j$$

Assuming to specify the treatment to the study of the motion of a satellite orbiting around the Earth, under the simplifying hypothesis of celestial bodies with spherical geometry and homogeneous and constant mass, in which we take into account only the contribution of gravitational forces, in accordance also with Newton's second law and knowledge to be able to bring back the acceleration vector $\mathbf{a}$ to the second derivative of the position vector $\ddot{\mathbf{r}}$, it is possible to write respectively for the Earth "1" and the satellite "2":

$$\ddot{\mathbf{r}}_1 = -G \sum_{j=2}^{n} \frac{m_j}{r_{j1}^3} \mathbf{r}_{j1} \tag{2.4}$$

$$\ddot{\mathbf{r}}_2 = -G \sum_{\substack{j=1 \\ j \neq 2}}^{n} \frac{m_j}{r_{j2}^3} \mathbf{r}_{j2} \tag{2.5}$$

By observing that:

$$\mathbf{r}_{12} = \mathbf{r}_2 - \mathbf{r}_1$$

$$\ddot{\mathbf{r}}_{12} = \ddot{\mathbf{r}}_2 - \ddot{\mathbf{r}}_1$$

Combining the previous equations, the result is:

$$\ddot{\mathbf{r}}_{12} = -G \sum_{\substack{j=1 \\ j \neq 2}}^{n} \frac{m_j}{r_{j2}^3} \mathbf{r}_{j2} + G \sum_{J=2}^{n} \frac{m_j}{r_{j1}^3} \mathbf{r}_{j1} \tag{2.6}$$

$$\rightarrow \ddot{\mathbf{r}}_{12} = -G \frac{m_1}{r_{12}^3} \mathbf{r}_{12} - G \sum_{j=3}^{n} \frac{m_j}{r_{j2}^3} \mathbf{r}_{j2} + G \frac{m_2}{r_{21}^3} \mathbf{r}_{21} + G \sum_{j=3}^{n} \frac{m_j}{r_{j1}^3} \mathbf{r}_{j1} \tag{2.7}$$

As $\mathbf{r}_{21} = -\mathbf{r}_{12}$, it can be written:

$$\ddot{\mathbf{r}}_{12} = -G \frac{m_1 + m_2}{r_{12}^3} \mathbf{r}_{12} - \sum_{j=3}^{n} G m_j \Big(\frac{\mathbf{r}_{j2}}{r_{j2}^3} - \frac{\mathbf{r}_{j1}}{r_{j1}^3} \Big) \tag{2.8}$$

2.3 Two-body Problem

Imagine studying the satellite motion compared to the other bodies present, neglecting the satellite mass, which is small compared to the other bodies in the system. It is possible to consider the restricted problem of n-body since the satellite does not exert gravitational force on the other bodies.

Instead, considering just one body that exerts its gravitational force on the satellite, it is possible to evaluate the two-body problem:

$$\ddot{\mathbf{r}}_{12} = -G \frac{m_1 + m_2}{r_{12}^3} \mathbf{r}_{12} \tag{2.9}$$

which neglecting satellite mass m_2 becomes:

$$\ddot{\mathbf{r}}_{12} = -G\frac{m_1}{r_{12}^3}\mathbf{r}_{12} \tag{2.10}$$

Finally, introducing the Standard gravitational parameter $\mu = Gm_1$, *the equation of motion* for the two-body problem will be:

$$\ddot{\mathbf{r}}_{12} = -\frac{\mu}{r_{12}^3}\mathbf{r}_{12} \tag{2.11}$$

2.3.1 Constant of Motion

Through scalar product for velocity vector $\dot{\mathbf{r}}$, the (2.11) is referable to a form in which the first term represents the kinetic energy for mass unity and the second term is the potential energy:

$$\varepsilon = \frac{v^2}{2} - \frac{\mu}{r} = \text{constant} \tag{2.12}$$

Since it has the size of an energy per unit mass, it is called specific mechanical energy. Introduced also the angular momentum:

$$\mathbf{h} = \mathbf{r} \times \mathbf{v} \tag{2.13}$$

to demonstrate the constant value along the trajectory is sufficient to multiply vectorially for $\mathbf{r}$ both members of (2.11), obtaining:

$$\mathbf{h} = \text{constant} \tag{2.14}$$

Moreover, since $\mathbf{h}$ is perpendicular to the plane containing the vectors velocity and position, it is easy to assume that the motion must necessarily take place on a plane, to which the trajectory of the satellite belongs and is called the orbital plane.

2.3.2 Trajectory Equation

Before analyzing the trajectory equation, let us introduce the concept of conic, that is, of the plane curve obtainable from the intersection of any plane with a two-pitch cone. Based on the intersection, a conic section can result in a circumference, an ellipse, a parabola, or a hyperbola, such as in the figure [fig 2.4]:

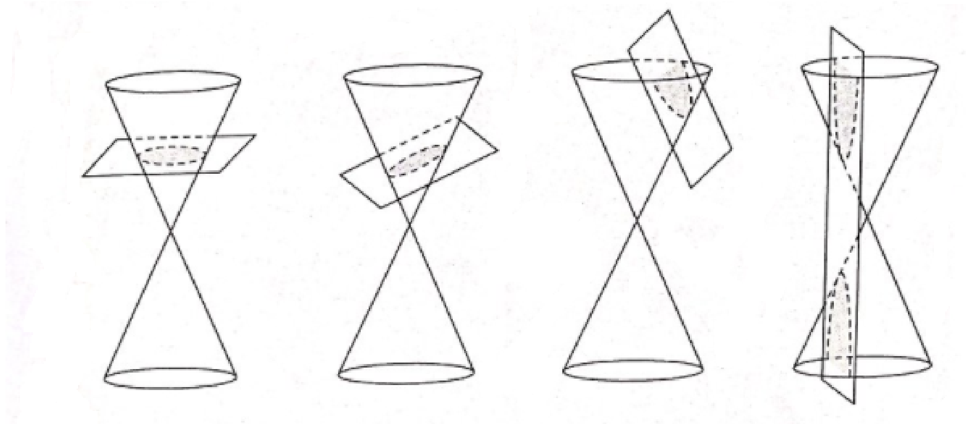

Figure 2.4: Conic Section

Defining a new parameter, the eccentricity e, as the ratio between a fixed point, called focus, on the plane of the conic and the distance from a fixed line, called the generator. Except for the parabola, it is defined as $e = \frac{c}{a}$ and according to its value we can classify:

Eccentricity	Conic Section
e=0	circumference
0<e<1	ellipse
e=1	parabola
e>1	hyperbola

Table 2.1: Conic classification based on eccentricity

The conics equation in polar form can be written as follows:

$$r = \frac{p}{1 + e \cos \nu} \tag{2.15}$$

in which true anomaly ν and semilatus rectum p appear. Through mathematical operations and solving the trajectory equation as a function of r can be shown that the two equations are comparable, so the trajectory in the problem of the two bodies can be a conic shape:

$$r = \frac{h^2/\mu}{1 + B/\mu \cos \nu} \tag{2.16}$$

2.3.3 Elliptic Orbit

For the ellipse, it is possible to identify several geometric parameters that allow a complete analysis. For orbits, in particular, depending on whether they are close to the main body or not, two points are distinguished, which are the periapsis and the apoapsis [fig 2.5].

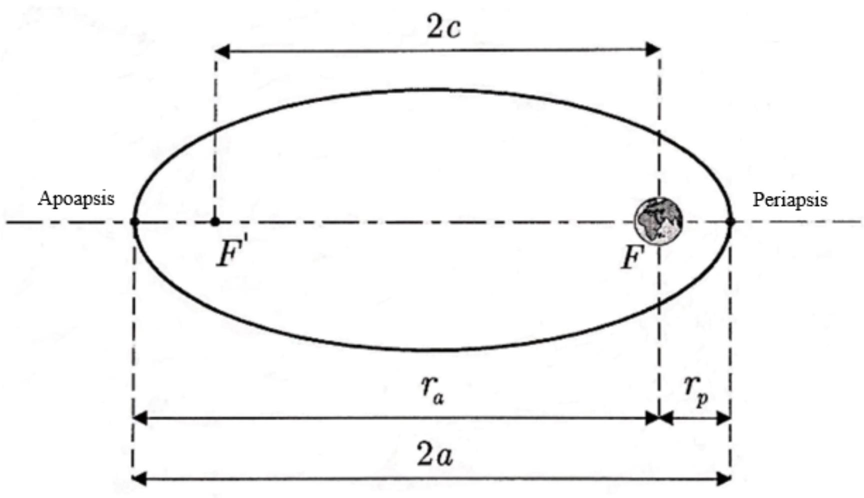

Figure 2.5: Geometric Elements of an elliptic Orbit

Through geometric properties, it is possible to determine the following relationships:

$$r_p = \frac{p}{1+e} = a(1-e) \tag{2.17}$$

$$r_q = \frac{p}{1-e} = a(1+e) \tag{2.18}$$

According to:

$$r_a + r_p = 2a$$

$$r_a - r_p = 2c$$

the eccentricity expression assumes the following form:

$$e = \frac{c}{a} = \frac{r_a - r_p}{r_a + r_p} \tag{2.19}$$

2.4 Classical Orbital Elements

Orbit characterization by the state vectors position and velocity alone turns out to be hardly intuitive, considering their temporal variation. In this regard, to uniquely identify the shape and size of the orbit, we consider six orbital parameters in the equatorial geocentric reference system, which are:

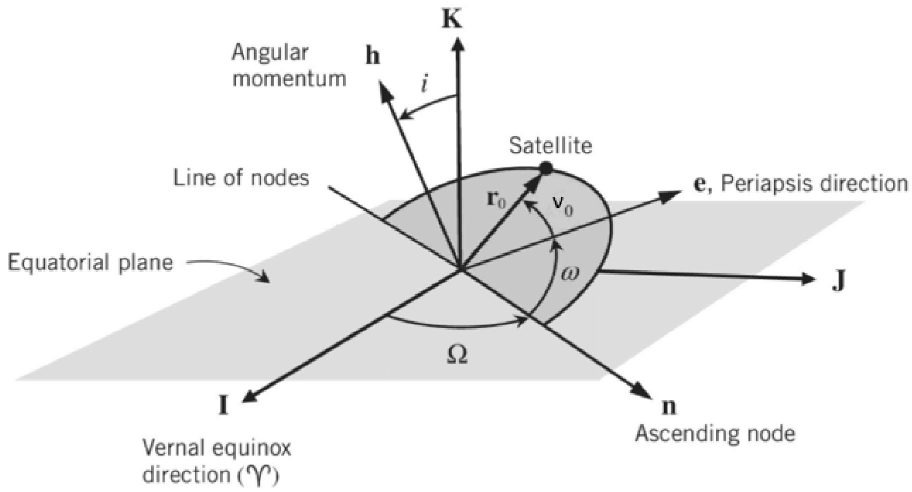

Figure 2.6: Definition of Keplerian Orbital Elements of a Satellite

- a - The semi-major axis fixes the size of the satellite orbit and goes from the center through a focal point to the edge of the ellipse. It can be considered the radius of the orbit at the periapsis and apoapsis, except in the circumference, where it coincides with the radius itself.

- e - The eccentricity defines the shape of the orbit, indicating the deviation of the orbit from a perfect circle.

- i - The inclination is the angle between the orbit plane and the equatorial plane, or between the z-axis of the equatorial-geocentric reference system and the direction w parallel to the angular momentum **h**. It takes increasing values counterclockwise from the equator itself.

- Ω - is the angle between the x-axis of the equatorial geocentric system and the direction $\hat{\mathbf{n}}$ indicating the line of nodes, given by the intersection of the orbital plane with the equatorial plane at the ascending node, which identifies the point at which the satellite passes from the southern to the northern hemisphere, unlike the descending node where the opposite occurs.

- ω - is the angle between the ascending node and the direction of the periapsis on the orbital plane, measured in the direction of the satellite's motion. Therefore, if the periapsis coincided with the ascending node, this angle would be equal to zero.
- ν - is the angle measured in the direction of motion from the eccentricity vector to the satellite's position at epoch time and indicates where the satellite is in its orbital path.

However, there are cases for which it is difficult to identify specific parameters. For example, for an eccentric equatorial orbit with i=0, not being able to define the line of nodes, we can introduce *longitude of periapsis* from the following relationship:

$$\pi = \Omega + \omega \tag{2.20}$$

Furthermore, when it is not possible to define in the perifocal plane of a circular orbit the periapsis, ω becomes undefined, and we can introduce *argument of latitude*:

$$u = \omega + \nu \tag{2.21}$$

Finally, in the case of equatorial circular orbits, since Ω and ω are indefinite, we introduce the time-dependent *true longitude*:

$$l = \Omega + \omega + \nu \tag{2.22}$$

2.5 Orbit Maneuvering

An orbital maneuver is the definition of the strategy to modify some parameters of a reference orbit by applying one or more propulsive actions. A fundamental part of the analysis of an orbital maneuver is evaluating the overall ΔV velocity change associated with it.[12]

2.5.1 Periapsis and Apoapsis Raising

To raise the apogee or perigee, keeping the radius unchanged, a variation of velocity is applied near the perigee in the first case or apogee in the second. Recalling the relationship between the energy and geometric orbit parameters it is possible to write that [13]:

$$\varepsilon = \frac{V^2}{2} - \frac{\mu}{r} = -\frac{\mu}{2a} \tag{2.23}$$

developing as a function of **v**:

$$V^2 = \frac{2\mu}{r} - \frac{\mu}{a} \tag{2.24}$$

The velocity change at the points where the impulse is given is equivalent to an increase in height at the opposite, such that it results in the following relations obtainable differentiating both members of the previous equation [fig 2.24]:

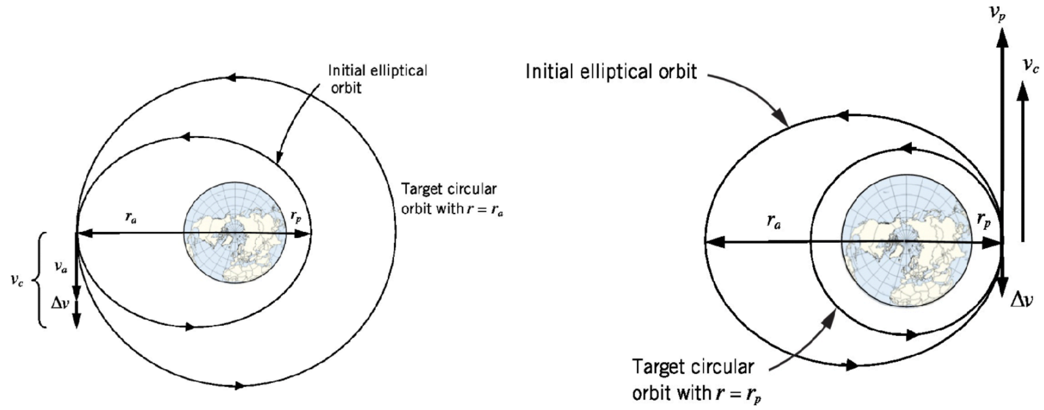

Figure 2.7: Example of Perigee Raising (left) and Apogee Raising (right)

$$\Delta h_a = \frac{4a^2}{\mu} V_p \Delta V_p \tag{2.25}$$

$$\Delta h_p = \frac{4a^2}{\mu} V_a \Delta V_a \tag{2.26}$$

2.5.2 Correction of Argument of Periapsis

To correct or change the value of the argument of the pericenter of an elliptical orbit, leaving unchanged the shape, of a given angle alpha fixed, you can make a maneuver at the points of intersection.

Since the orbit is constant, the vector **h** angular momentum is the same for the two orbits, so the absolute velocity of the satellite does not change during the maneuver, but the direction of the vector **v** undergoes only a rotation equal to an angle 2γ. The final ΔV will be given by:

$$\Delta V = 2\sqrt{\frac{\mu}{a(1-e^2)}} e \sin\left(\frac{\alpha}{2}\right) \tag{2.27}$$

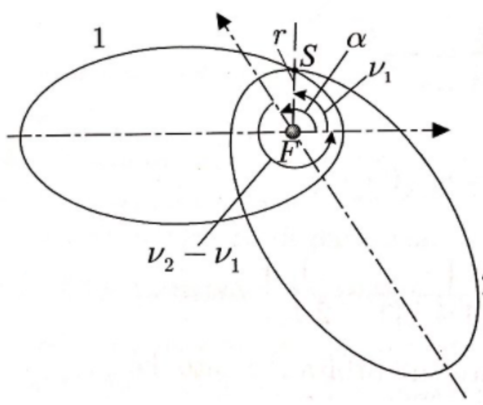

Figure 2.8: Change in Argument of Periapsis

2.5.3 Simple Plane Change

it is possible to change the orientation of the orbital plane by providing a velocity increment with a component normal to the orbit plane. Thus, there will be a change in the inclination and longitude of the ascending node.

To change just the inclination of a given value of θ, it is necessary to burn near the ascending or descending node when the satellite crosses the equatorial plane. The required change in velocity is obtained by using the law of cosines:

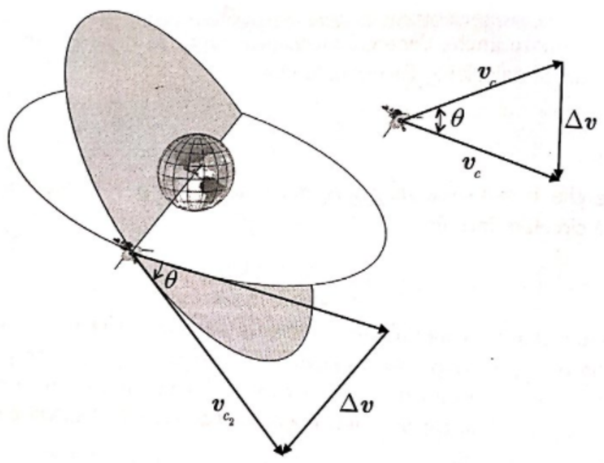

Figure 2.9: Plane Change for Circular Orbit

$$\Delta V = 2V_c \sin\left(\frac{\theta}{2}\right) \tag{2.28}$$

where V_c indicates the orbital velocity. In the maneuvering strategies that include orbital transfers through, for example a Hohmann, it is possible to perform the inclination change at the apogee of the transfer orbit, where the satellite speed is minimal, decreasing the energy cost of the maneuver itself.

2.5.4 Hohmann Transfer

To perform a two-impulse maneuver, it is necessary to consider the Hohmann transfer, which allows transfer between two co-planar orbits by a semi-elliptical trajectory tangent to both at the periapsis and apoapsis. The final ΔV will be

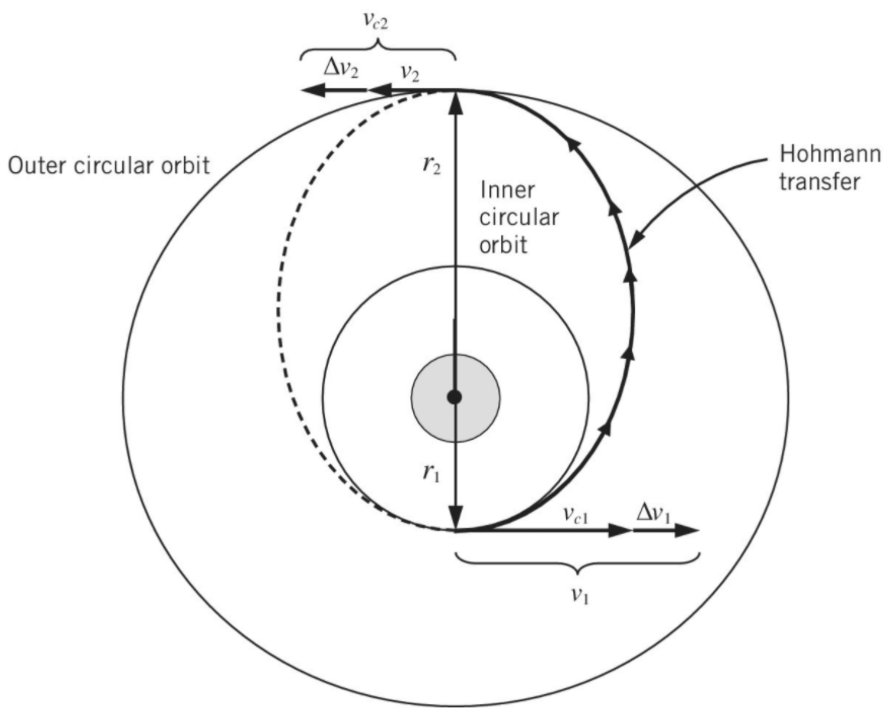

Figure 2.10: Hohmann Transfer Showing Orbit Transfer Between Two Circular, Co-planar Orbits

given by the sum of the individual ΔV in which, starting from the initial orbit and considering the orbital velocity it is necessary to provide an impulse to begin the transfer, such that:

$$V_{c1} + \Delta V_1 = V_{h1} \tag{2.29}$$

where V_{h1} is the velocity of transfer orbit at the periapsis. it is possible to obtain its value from the energy conservation equation and then calculate ΔV_1. At the apoapsis, it is possible to apply similar reasoning such that:

$$V_{c2} = \Delta V_2 + V_{h2} \tag{2.30}$$

The total ΔV_{tot} will be:

$$\Delta V_{tot} = |\Delta V_1 + \Delta V_2| = |V_{h1} - V_{c1}| + |V_{h2} - V_{c2}| \tag{2.31}$$

$$\Delta V_{tot} = V_{c1}\left(\sqrt{\frac{2r_2}{r_1 + r_2}} - 1\right) + V_{c2}\left(1 - \sqrt{\frac{2r_1}{r_1 + r_2}}\right) \tag{2.32}$$

Since the delta-V are parallel to the velocities, there will be no misalignment losses. In addition, by thrusting horizontally, it is possible to neglect gravity losses as well. It represents the most economical transfer from the energy point of view, requiring a minimum change in speed, but at the same time the longest in terms of time, calculated as half the period associated with the elliptical transfer orbit (T_E):

$$\Delta t_h = \frac{T_E}{2} = \pi\sqrt{\frac{a_H^3}{\mu}} \tag{2.33}$$

Chapter 3

Electric Propulsion

Over the past two decades, there has been an increase in the design and use of spacecraft with low-thrust engines with high exhaust velocities and higher energy density per unit mass. Because the effective thrust, compared to chemical propulsion, turns out to be lower, longer thrust times are required before high-velocity changes are achieved.

An increasing number of satellites around Earth use low-thrust propulsion for station keeping and orbit raising. To be able to make the correct assumptions to design low-thrust trajectories, a basic understanding of low thrust is required.[14] The provision of low values of thrust in a continuous manner resulting in variations of the orbital elements during the maneuver itself makes the study of this type of maneuvers more difficult than impulsive ones.

3.1 Edelbaum Approximation

To obtain analytical solutions for electric propulsion, it is necessary to reformulate the already known Gauss planetary equations that describe the temporal variations of the orbital parameters considering the effects of the same.

The problem of low-thrust optimal transfer between inclined circular orbits was presented by Edelbaum in the early 1960s. Consider the following simplifying assumptions, such as:

- Considering circular or nearly circular orbits ($e \approx 0$), it is possible to approximate the semi-axis with the orbital radius at each point, such that $r \approx a \approx p$, $V^2 \approx \frac{\mu}{r}$, $E \approx \nu \approx M$
- A small orbital inclination is considered ($i \approx 0$), such that choosing as reference plane that of the initial orbit, it can be written $\cos i \approx 1$ and $\sin i \approx i$
- Small thrust and acceleration components, such that $\frac{T}{m} << \frac{\mu}{r^2}$

Imagining also to be able to define in the orbital plane three components of acceleration, valid as reference directions, parallel to the velocity (a_t), a centripetal acceleration to the trajectory (a_r) and one outside the plane (a_w), the Gauss equations will be:

$$\dot{a} = \frac{2ra_t}{V} \tag{3.1}$$

$$\dot{e} = \frac{1}{V}(2\cos\nu a_t - \sin\nu a_r) \tag{3.2}$$

$$\dot{i} = \frac{a_w}{V}\cos(\omega+\nu) \tag{3.3}$$

$$\dot{\omega} = \frac{1}{eV}\Big(-V\frac{d\Omega}{dt} + 2\sin\nu a_t - \cos\nu a_r\Big) \tag{3.4}$$

$$\dot{\Omega} = \frac{a_w}{iV}\sin(\omega+\nu) \tag{3.5}$$

$$\dot{\theta} = \dot{M} = \dot{\nu} = \sqrt{\frac{\mu}{r^3}} \tag{3.6}$$

According to the previous assumptions, in circular orbits, a singularity arises since the periapsis and ascending node are not defined. Therefore Edelbaum considers the only equations that do not contain these parameters, (eq 3.1), (eq 3.2), (eq 3.3). Moreover, it is possible to explicate the accelerations such as a thrust function, according to given angles, along with the three directions of acceleration, obtaining:

$$a_t = \frac{T}{m}\cos\alpha\cos\beta \tag{3.7}$$

$$a_r = \frac{T}{m}\sin\alpha\cos\beta \tag{3.8}$$

$$a_w = \frac{T}{m}\sin\beta \tag{3.9}$$

Depending on the orbital parameter of which the variation is required, the optimal direction of acceleration will be determined.

It makes sense to think that pushing parallel to the speed will result in a variation of the semi-axis, burning radially in the plane will generate apses rotation, and burning out of the plane will result in a variation of inclination. However, it is useful to understand how can be manipulated the accelerations to vary a single orbital parameter, if required, keeping the others unchanged.

1. To change only the semi-axis and keep the eccentricity unchanged after a complete revolution, it is necessary to push with $\alpha = \beta = 0$, compliance or not with the motion according to whether you want to increase or decrease Δa.

2. The simple plane change is instead obtained by thrusting out of the plane with $\beta = \pm\frac{\pi}{2}$ positive or negative depending on whether it is desired to increase the inclination and therefore the latitude or vice versa.

3. To change instead only the eccentricity, it is sufficient to push with $\beta = 0$ and with $\tan\alpha = \frac{1}{2}\tan\theta$, whose trend resembles that of $\alpha = \theta$, that can be demonstrated by setting to zero the derivative of the eccentricity as a function of time and evaluating the maximum. By doing so, first of all, a variation of the semi-major axis will occur, but it will get zero in the following revolutions. It is, therefore, a matter of thrusting in a fixed direction in space and obtaining the maximum possible change in eccentricity.

Finally, to obtain a combined variation of inclination and semi-axis, leaving unchanged the eccentricity, it is pushed with $\alpha = 0$ and with a beta angle such as to obtain $\tan\beta = \cos(\theta)k$. However, to obtain sensitive results, it is necessary to consider more revolutions and to understand which beta value to assume depending on the radius of the orbit considered, Edelbaum proposed to consider always near-circular orbits, even those of transfer, which allows to exploit the results obtained for a single revolution and to have a constant thrust angle for each revolution. The analysis, conducted using the ΔV as an independent variable, leads to the following result:

$$V\sin\beta = V_0\sin\beta_0 = \text{constant} \tag{3.10}$$

Being constant the product between the sine of the thrust angle and the velocity it will be had that where the velocity is large there will be small β, and vice versa when the velocity is smaller.
In general, it is possible to tabulate the characteristic velocities for small variations of the parameters:

Delta-V	Low-Thrust
ΔV_a	$0.5\frac{V}{r}\Delta a$
ΔV_e	$0.649\Delta e$
ΔV_i	$\frac{\pi}{2}V\Delta i$

Table 3.1: Delta-V for orbital variations

3.2 Coplanar Circle-to-Circle Transfer

Given low and continuous thrust, a maneuver with electric propulsion follows a spiral trajectory that takes place when starting from a circular orbit. The near-circular nature of the low-thrust spiral transfer allows analytical solutions to be determined. Assume that the thrust is always aligned with the velocity vector, neglecting the radial and out-of-plane acceleration components.

It is possible to show how the semi-major axis and eccentricity remain constant for few revolutions, without altering the energy of the orbit and thus the shape. These assumptions then allow considering a nearly circular spiral trajectory [fig 3.1].

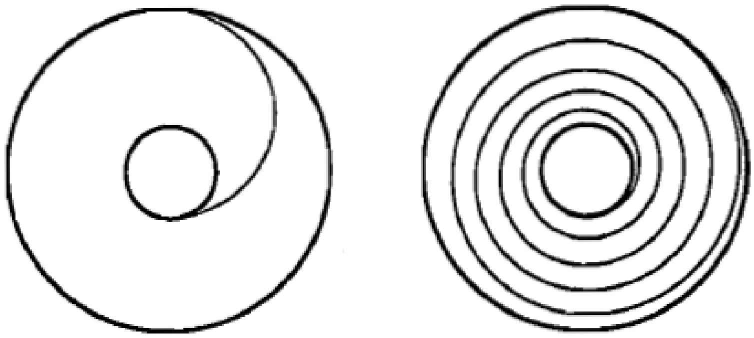

Figure 3.1: Hohmann Transfer (left) and Low-Thrust Spiral Transfer (right)

From the previous analysis, it is possible to calculate the transfer time and then the calculation of the propellant mass necessary for the maneuver, assuming to operate with a constant mass-flow rate:

$$t_f = \tau \left[1 - \exp\left(\frac{-\Delta V}{c} \right) \right] \tag{3.11}$$

where $\tau = m_0/\dot{m}$ is the initial spacecraft mass divided by the engine mass-flow rate and the ΔV is given by the difference between the orbital velocity of the initial and final orbit:

$$\Delta V = |V_i - V_f| \tag{3.12}$$

3.3 Inclination Change

In a pure plane change, the thrust vector is always normal to the orbital plane. In such a case, the thrust components along the velocity and plane normal directions are zero, and thus the semi-major axis and eccentricity remain constant.

By integrating the Gauss equation on the variation of the inclination along the orbit and then dividing it by the orbit period, it is possible to find the average rate of variation of the inclination, which can be exploited to estimate the variations of the parameter after many orbital revolutions. Similarly to the previous case, it is possible to find the time of the maneuver according to the relation:

$$t_f = \tau \Big[1 - \exp\Big(\frac{-\Delta i \pi V}{2c} \Big) \Big] \tag{3.13}$$

where Δi is the magnitude of the desired plane change in radians. The low-thrust ΔV for a pure inclination change is:

$$\Delta V = \frac{\Delta i \pi V}{2} \tag{3.14}$$

Decoupling the changes in the orbital elements allowed us to solve the Gauss variational equations using variable separation and analytical integration. Edelbaum obtained a closed-form solution for the general three-dimensional low-thrust transfer between inclined circular orbits, where the out-of-plane acceleration component must vary optimally to make most of the change in inclination occur at higher orbital altitudes.

The main result for the increase in velocity for a low-thrust transfer between two orbits with a change in inclination is provided by the following relationship:

$$\Delta V = \sqrt{V_0^2 + V_f^2 - 2V_0 V_f \cos\Big(\frac{\Delta i \pi}{2} \Big)} \tag{3.15}$$

whose corresponding maneuvering time is therefore given by:

$$t_f = \tau \Big[1 - \exp\Big(\frac{-\Delta V}{c} \Big) \Big] \tag{3.16}$$

Chapter 4

Mission Analysis

The purpose of this chapter is to identify the optimal orbit that will allow biodiversity study of the species thanks to Earth Observation.

The maneuvers necessary to bring the satellite into operational orbit and to ensure its orbital maintenance, subject to the various perturbations and the eventual de-orbiting maneuver depending on the operational life of the satellite, by the guidelines established by European Space Debris Safety and Mitigation Standard, will be taken into account.

In the field of remote sensing, sun-synchronous orbits have found important developments that allow covering in a capillary way all the terrestrial areas, ensuring a reduced use of the number of co-located satellites in the constellations.

4.1 Orbit Selection

Sun-Synchronous orbits have the peculiarity of having an orbital plane that maintains a fixed orientation relative to the sun during all periods of the year. In other words, $\dot{\Omega}$ is chosen to equal the average speed with which the sun, in its apparent motion around the earth, moves on the celestial sphere. It can therefore be written that:

$$\dot{\Omega} = -\frac{3}{2} J_2 \sqrt{\frac{\mu_e}{a^7}} \frac{R_e^2}{(1-e^2)^2} \cos i = \dot{\Omega}_{elio} \tag{4.1}$$

Since the orbit is retrograde, the negative term associated with the cosine turns the derivative of omega positive. In this way, the line of the nodes rotates on the equatorial terrestrial plane in a counterclockwise direction (proceeds) and the orbital plane follows the apparent rotation of the Sun on the celestial sphere.

Therefore, satellites in Sun-Synchronous orbits have the same local time on the same latitude in the ascending (or descending) section of each revolution, the second is that the angle between the solar ray and the orbital plane varies slightly and is not significant.

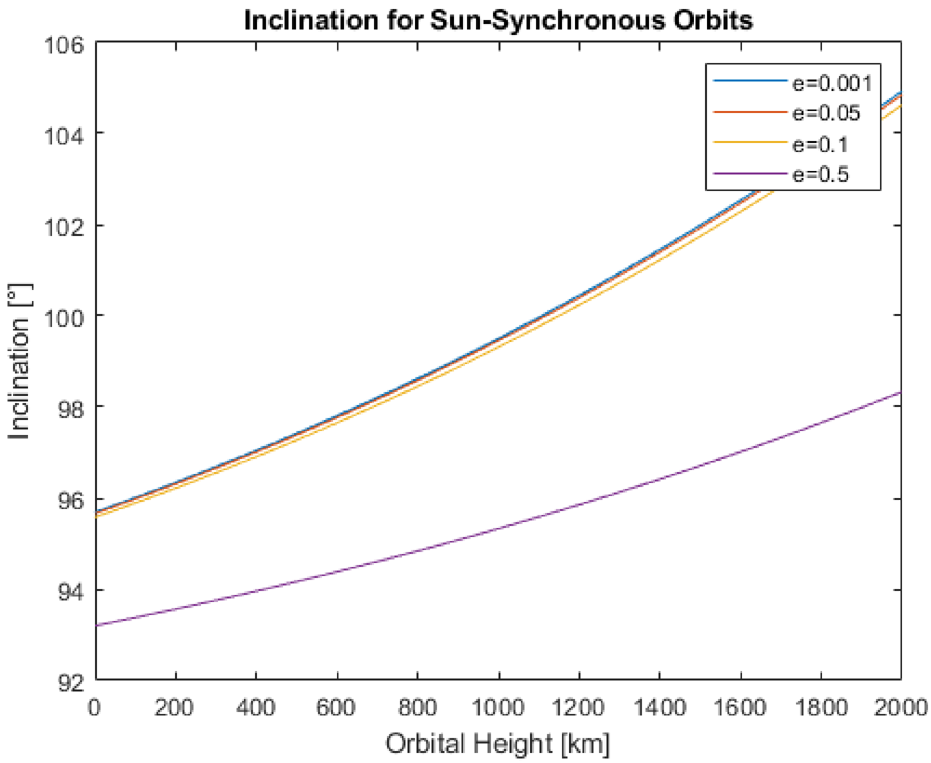

Figure 4.1: Necessary Inclination to obtain Sun-Synchronous orbit from given Orbital Height

The Sun-Synchronous orbit can put a satellite in a more stable illumination due to these two features, which are conducive to the satellite energy, thermal control, and attitude control, thus reducing the complexity of the satellite system and favoring the optical imaging of Earth observation. In practice, the solar synchronous orbit with Local Time of Descending Node (LTDN) at 10:30 and 13:30 are mostly used by optical remote sensing satellites, which is in line with what is imposed by mission constraints.

At the same time, the characteristics associated with frozen orbits can also be considered. The frozen orbit refers to the orbit whose change rate of the argument of perigee and eccentricity are both zero and is not limited to a specific inclination. For LEO satellites, there are two possibilities for the corresponding frozen orbit, that is, orbits with an argument of perigee $\omega = 90°$ or $\omega = 270°$.If the semimajor axis of and the inclination of the orbit are given, the corresponding frozen orbit eccentricity can be uniquely determined according to:

$$e = -\frac{J_3 \sin i}{J_2 \cdot 2p} \tag{4.2}$$

Satellites on frozen orbit are at constant altitude when passing through the same latitude area at different times. With this feature, the image scale can be obtained by remote sensing satellites to be consistent, thus facilitating the stitching and comparison of images at different times, and playing a core role in Earth observation [15].

To ensure consistency in data analysis, satellites involved in earth observations are placed in orbits such that the satellite repeats its path after a fixed time interval. This time interval is called the satellite repeat cycle.

For a track to be retraced there must be a periodic rephasing of the motions of the satellite and the Earth, i.e. a periodic reproduction of the same situation between the two; that is the periodic rephasing of the satellite over a given location with the same direction of motion.

This can happen every R orbits of the satellite and N days (nodal) if the equality of the two times R T_{sat} and N G_{nod} is verified where T_{sat} is the period of the satellite and G_{nod} is a day (nodal, to be precise). The condition of repetitiveness is:

$$R\ T_{sat} = N\ G_{nod} \tag{4.3}$$

where R is the total number of revolutions in N nodal days [16].
According to the mission requirements, considering a variable orbital altitude between 470-550 km and predetermined the number of nodal days ($\sim$ 14 nodal days) for circular orbit, obviously knowing also the duration of a single nodal day, it was possible to proceed in the choice of an orbit that combined the characteristics of Sun-Synchronous and repetitiveness orbit.

From the previously mentioned parameters, it is possible to derive the number of total orbits to be performed on the nodal days. However, since the result returns a non-integer number, it was necessary to round up to the nearest one and from it calculate a new value for an orbital period and therefore of the semi-major axis (a). Finally, these values were then reused for the calculation of the optimal inclination from [eq 4.1] such as to make the Sun-Synchronous orbit. The analysis led to the following orbits:

These analyses were supported through the use of System Tool Kit (STK) software for visualization and subsequent simulations for evaluations of coverage times of areas of interest and accesses on the specified stations.

Solutions	Altitude[km]	Inclination [°]	Eccentricity	Revolutions [R]
1st	474.066	97.3087	≈ 0	214
2nd	495.543	97.3896	≈ 0	213
3rd	517.188	97.4718	≈ 0	212
4th	539.004	97.5553	≈ 0	211

Table 4.1: Conditions for Sun-Synchronous and recursive orbits

4.2 Mission Phases

Following evaluations of Vega missions, the mission of VV16 has been taken as reference, for which it has been assumed to release the DANT-e satellite through a piggyback launch in a Sun-Synchronous orbit at 515 km with an inclination of 97.45°.For the DANTe-1 mission the following phases has been identified:

- *Launch and Early Orbit Phase* (LEOP): The launch and early orbit phase can be divided into the following sub-phases:
  - Countdown and launch, which last from the beginning of countdown over the lift-off till the separation of the spacecraft from the launch vehicle.
  - acquisition phase, which starts after separation of the spacecraft from the last stage of the launcher.

  At the separation the satellite is automatically powered and the attitude of the spacecraft is controlled in order to damp the angular velocity generated by the launcher injection and to reach a safe sun pointing attitude. At the first visibility with the VHF/UHF band station the communication link is acquired.

- *Commissioning phase*: After completion of the LEOP the commissioning phase can start. In this phase all the platform and payload functionalities and mode are exercised and validated.

- *Operational phase*: Once the commissioning phase is completed the satellite and the ground segment are fully operational in nominal conditions. The main task to be performed during the operational phase is the hyperspectral images acquisition and processing.

- *Emergency phase*: In case an anomaly occurs during any of the above mission phases, the spacecraft could enter in emergency phase, the satellite is brought in a safe configuration in order to ensure its survivability. The on-board data are analysed to understand the source of the anomaly and the corrective actions are actuated. Once the satellite recovers its full functionality, the operational phase can be restarted.

- *Disposal phase*: After the end of the mission lifetime the satellite is set in a safe configuration and remains in stand-by (the satellite will not perform any communication with ground). The de-orbiting duration compatible with the maximum permitted by the European Space Debris Safety and Mitigation Standard (i.e. 25 years) is guaranteed.

4.3 Operational Orbit

Once LEOP operations in the parking orbit for the on-board instrumentation check have been completed and the possibility of communication with ground stations has been verified, it is necessary to change the altitude and inclination of the satellite to reach the operational orbit, where the nominal phase for the acquisition of earth data can begin.

For orbital transfers and stationkeeping maneuvers to ensure the maintenance of the orbital altitude within certain levels, an electric thruster (*Regulus Enanched Plasma Thruster*) has been considered as requested by S.A.B. Aerospace in collaboration with T4i (Tecnhnology for Propulsion and Innovation), whose characteristics are reported in [tab 4.2] below:

Thrust	0.25 – 0.65 mN
Specific Impulse	Up to 650 s
Input Power	20 - 60 W
Mass flow	0.1 mg/s
Propellant	Iodine
Volume	1.5 U (93.8 x 95.0 x 151.0 mm)
Weight	2.5 kg

Table 4.2: Regulus Characteristics

The ΔV associated with the maneuvers described were calculated for the different options evaluated in the [tab 4.1], referring to the [eq 3.11] and [eq 3.12] for low-thrust simple orbital transfer. The results are as follows:

Solutions	Altitude[km]	Inclination [°]	ΔV [m/s]	transfer time [d]
1st	474.066	97.3087	22.7	8.22
2nd	495.543	97.3896	10.8	3.90
3rd	517.188	97.4718	1.2	0.44
4th	539.004	97.5553	13.2	4.79

Table 4.3: ΔV for low-thrust co-planar transfer

From this table, it is possible to evaluate an optimal solution as a function of minimum energy cost and reduced transfer time. For the calculation of the energy cost, it has already been taken into account to consider a change of plane in the operational orbit in case of orbital raising to minimize the cost given a reduced orbital velocity, or vice versa, if a decrease in orbital altitude is necessary the calculation has been made on the parking orbit. Proceeding with the calculation of the maneuvering cost associated with a plane change, concerning [eq 3.13] and [eq 3.14] the following results are obtained:

Solutions	Altitude[km]	Inclination [°]	ΔV_i [m/s]	transfer time [d]
1st	474.066	97.3087	29.46	10.7
2nd	495.543	97.3896	12.59	4.57
3rd	517.188	97.4718	4.54	1.65
4th	539.004	97.5553	21.91	7.94

Table 4.4: ΔV for low-thrust inclination change

From these observations, it is easy to see that it is possible to be able to make the satellite operational within two weeks, with costs in terms of ΔV contained. However, it is possible to reduce the ΔV cost and transfer time by exploiting the combined maneuvering between inclined orbits, as seen in [eq 3.15] and [eq 3.16], obtaining:

Solutions	Altitude[km]	Inclination [°]	ΔV_c [m/s]	transfer time [d]
1st	474.066	97.3087	37.21	13.47
2nd	495.543	97.3896	16.57	6.01
3rd	517.188	97.4718	4.70	1.71
4th	539.004	97.5553	25.60	9.28

Table 4.5: ΔV for Combined Maneuvers

As a first estimation, it is easy to see that in terms of cost, the third solution represents the optimal one. Before continuing the analysis by evaluating the efficiency of each orbit from the point of view of coverage, it is good to remember which perturbations are involved in the orbital alterations and how they influence ΔV in orbital maintenance.

4.4 Orbit Perturbations

The two-body problem and the restricted two-body problem presented above describe the ideal orbit of a body around the Earth. In practice, the satellite orbit is perturbed by numerous secondary effects, which cannot always be neglected.In the case of LEO orbits, the two most prominent perturbative phenomena are generally the drag and the non-perfect sphericity of the Earth.

Aerodynamic drag modeling is crucial for orbit specification and prediction since it results in a drag force on the satellite leading to energy dissipation and leading to a reduction in orbital period and height. At lower heights, increasing densities are encountered, accelerating orbital decay. The acceleration due to drag can be calculated as follows:

$$a_D = -\frac{1}{2}\rho\frac{C_D A}{m}V^2 \tag{4.4}$$

where ρ is the local atmospheric density, C_D is a dimensionless drag coefficient normally ≈ 2.2 for low-orbit satellites, A is the spacecraft area projected along the direction of motion, V is the relative velocity of the spacecraft with respect to the atmosphere and m is the satellite mass. The above considerations led to the choice of a frozen sun-synchronous orbit with a repetitive track, whose orbital parameters are very stable and not subject to perturbing forces, making it possible to neglect variations in eccentricity and evaluate only those relative to the semi-major axis. The variations of i and Ω subject to aerodynamic resistance are zero since they depend only on the component of the perturbation force normal to the orbital plane.So for each orbit we will have, given the near-circular orbit:

$$\Delta a_{rev} = -2\pi \frac{C_D A}{m} \rho a^2 \tag{4.5}$$

It will be necessary to consider an additional cost in terms of ΔV for proper orbital maintenance according to table 3.1, such that:

Solutions	Altitude[km]	Δa_{rev} [m]	ΔV (1 year) [m/s]
1st	474.066	7.02	16.36
2nd	495.543	3.53	10.85
3rd	517.188	2.69	8.18
4th	539.004	1.84	5.54

Table 4.6: ΔV for low-thrust station-keeping

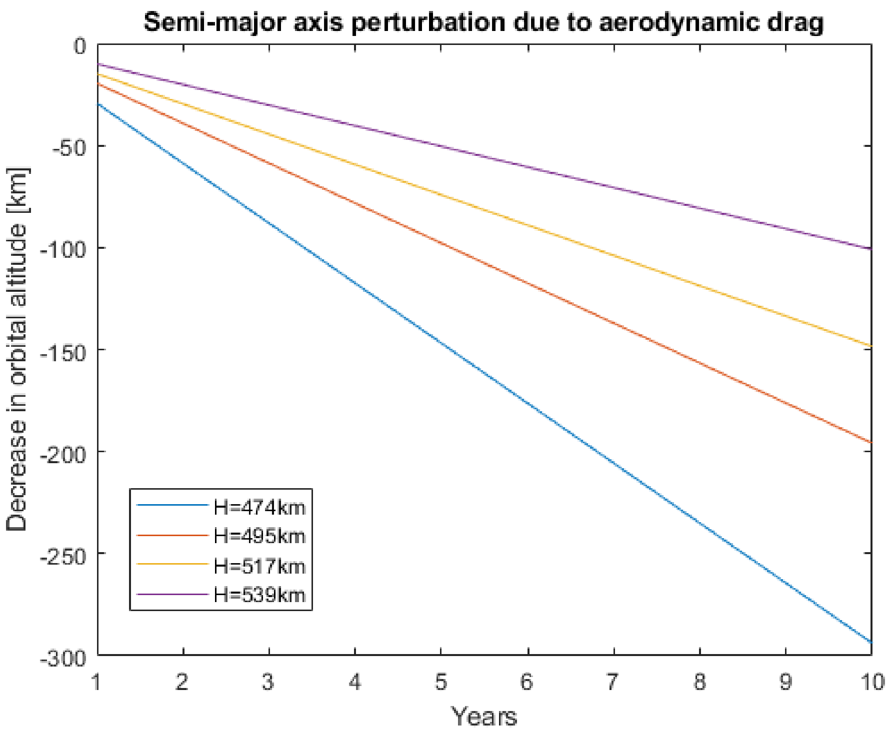

Figure 4.2: Semi-Major Axis degradation in 10 years [km]

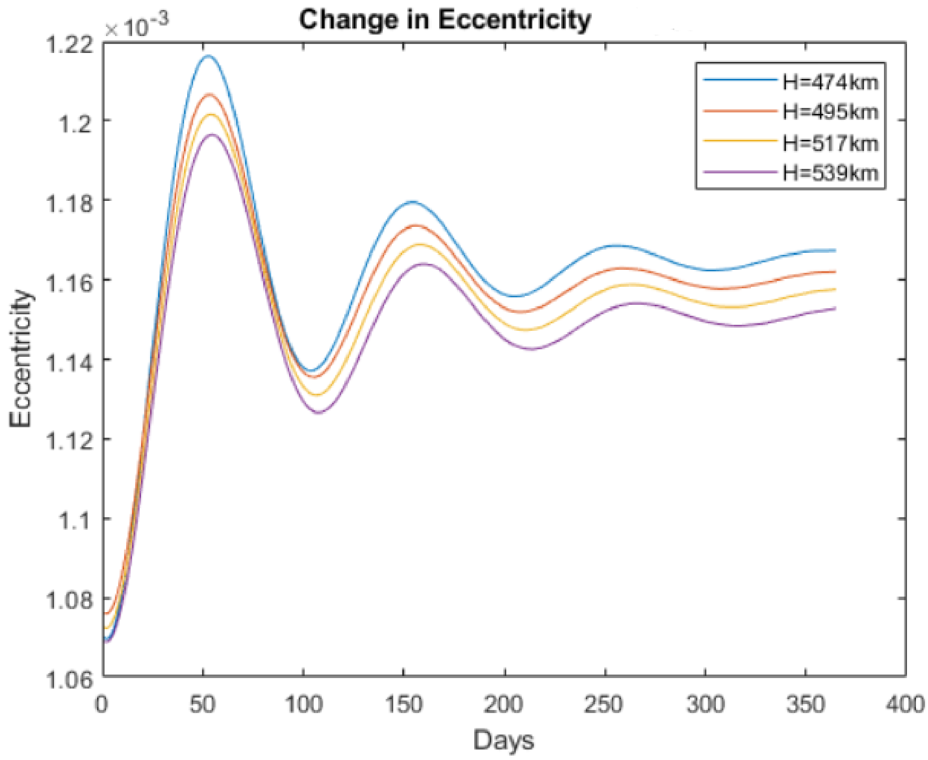

Figure 4.3: Orbital Parameter - Eccentricity

In particular, from the variations of the semi-major axis for each orbit, it is easy to evaluate the daily displacement by considering the number of revolutions of the satellite for each day. In addition, to prevent it from failing to meet the coverage requirements for the areas of interest, a margin of error of about ≈ 2 km will be considered below which the correction maneuvers will be carried out.

The Earth's gravitational field, given the Earth's non-sphericity, is generally modeled by associating it with the shape of a geoid, which allows effects such as the flattening of the poles to be taken into account, whose gravitational potential can be expressed as follows:

$$U = \frac{GM}{r}\left[1 - \sum_{n=2}^{\infty}\left(\frac{R}{r}\right)^{n} P_n(\sin\delta)\right] \tag{4.6}$$

with r being the distance of P from the centre of mass of the body, M and R indicating the mass and equatorial radius of the earth, δ being the declination, P_n being the polynomial of Legendre and finally J_n indicating an appropriate dimensionless coefficient, subsequently classified as a zonal harmonic [17].

For the study of perturbations, only J_2, which is responsible for the flattening of the poles, will be taken into account, as it is larger than the others. It affects the *right ascension of the ascending node* and *argument of perigee*. In both cases, the rate of change for day is given by the following relationships:

$$\dot{\Omega} = -3\pi J_2 \left(\frac{R}{p}\right)^2 \cos(i) n_0 \tag{4.7}$$

$$\dot{\omega} = \frac{3}{2}\pi J_2 \left(\frac{R}{p}\right)^2 (5\cos^2(i) - 1) n_0 \tag{4.8}$$

expressed in $[rad/day]$ with n_0 indicating the number of daily revolutions of the satellite. In the case of the selected orbits, however, since they are Sun-Synchronous and therefore exploit this effect to maintain a fixed orientation to the sun, a certain daily rotation of the node line is required, which is not compensated by station-keeping.

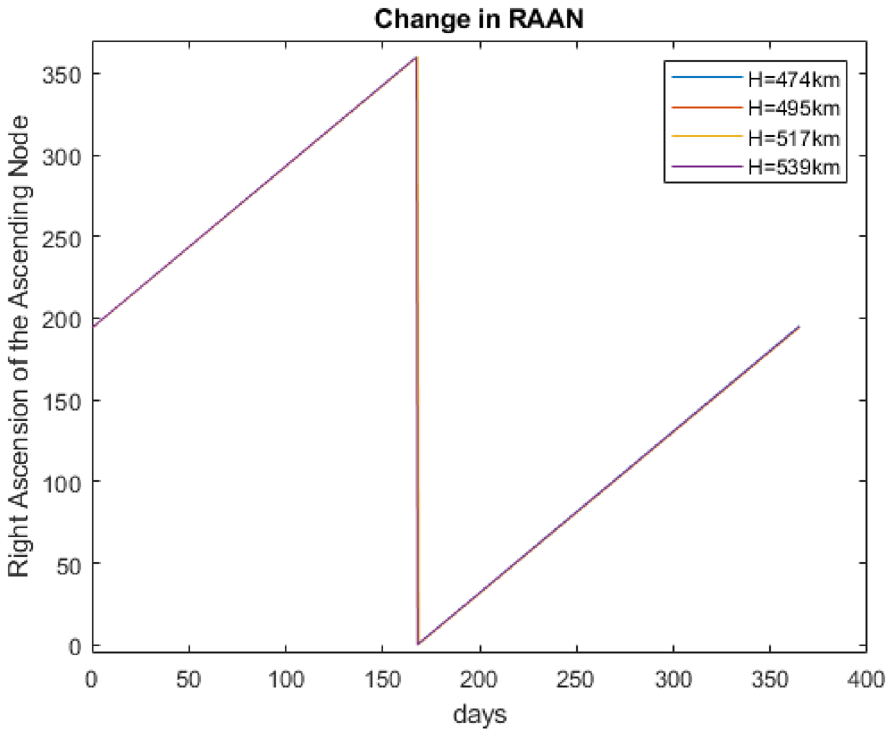

Figure 4.4: Orbital Parameter - RAAN

Furthermore, since the eccentricity value is ≈ 0, the variation associated with the argument of perigee is practically negligible.

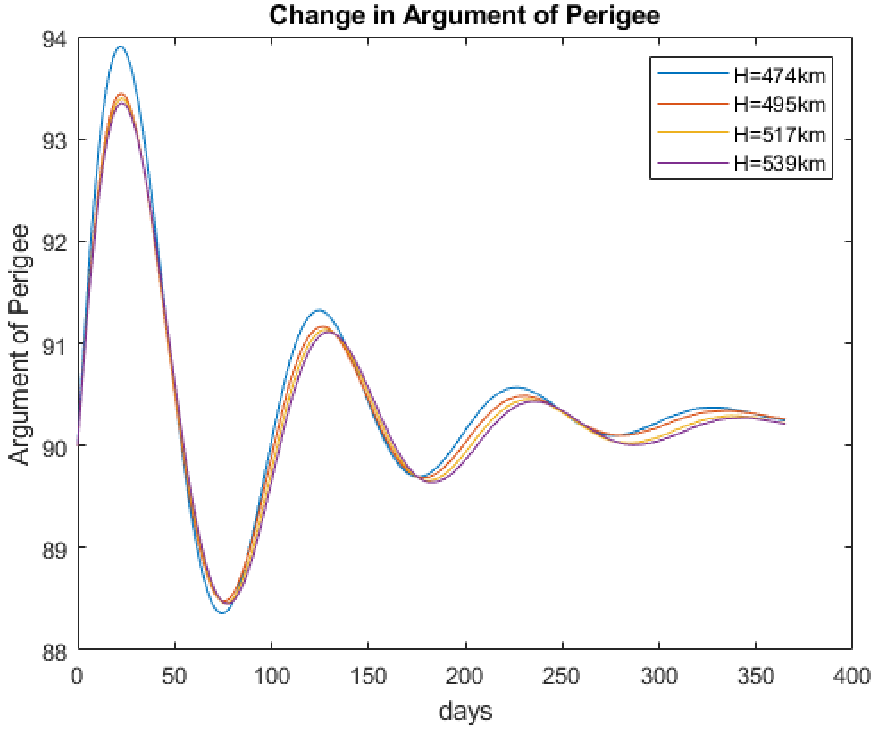

Figure 4.5: Orbital Parameter - Argument of Perigee

4.5 Disposal and ΔV Budget

To comply with the provisions of the European Space Debris Safety and Mitigation Standard for the maximum operational life of the satellite, it is essential to also take into account any de-orbiting operations. In this regard, starting from the standard atmosphere model, entering the satellite parameters including the area exposed to the sun and the aerodynamic drag, as well as the initial mass, the satellite lifetime was calculated using STK for the different solutions:

	474.066	495.543	517.188	539.004
Lifetime [years]	8	11.6	17.2	25.2

Table 4.7: Satellite Lifetime - Standard Atmospheric Model 1976

Except for the solution at H=539 km, which involves additional disposal maneuvers to lower the operational altitude and speed up orbital decay, the other orbits are within the established operational limits.

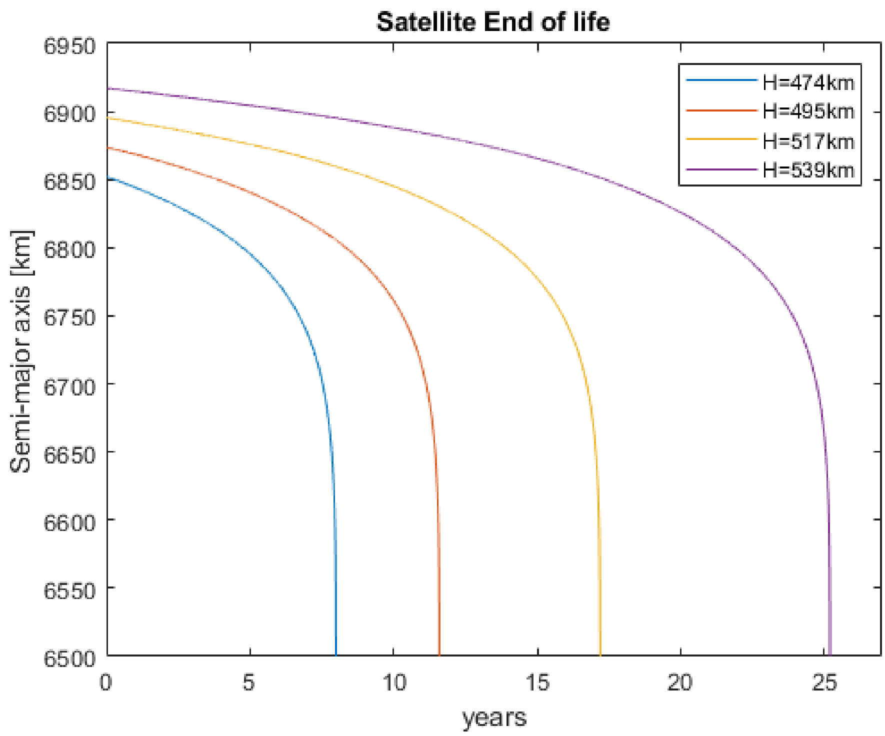

Figure 4.6: End of Life

Although for altitudes below 500 km it is necessary to contemplate further measures to extend the operative life, initially set for 5 years. Following these considerations, it is possible to estimate the ΔV needed for the whole mission, including the transfer and station keeping maneuvers for the different cases analyzed. The following margins have to be considered for each maneuver, covering the uncertainties in the mission design and the system performance [18]:

- R-DV-11: 5% for accurately calculated manoeuvres (trajectory manoeuvres as well as detailed orbit maintenance manoeuvres)
- R-DV-12: 100 % for general (not analytically derived) orbit maintenance manoeuvres, over the specified lifetime (maintenance manoeuvres calculated in detail shall be handled according to R-DV-11)

Solutions	ΔV Maneuvers	ΔV Maintenance	ΔV_{tot}
1st - 474 km	39.07 m/s	163.6 m/s	202.67 m/s
2nd - 495 km	17.41 m/s	108.5 m/s	125.91 m/s
3rd - 517 km	4.94 m/s	81.8 m/s	86.74 m/s
4th - 535 km	26.88 m/s	55.4 m/s	82.28 m/s

Table 4.8: ΔV budget

Since changes in inclination are in the order of a hundredth of a degree, so much so that during the whole operating life there is a $\Delta i = 0.55$ degrees, and considering that the satellite can be decommissioned before that time, it can be stated that variations in the short term are negligible and therefore for this effect a real corrective ΔV is not considered.

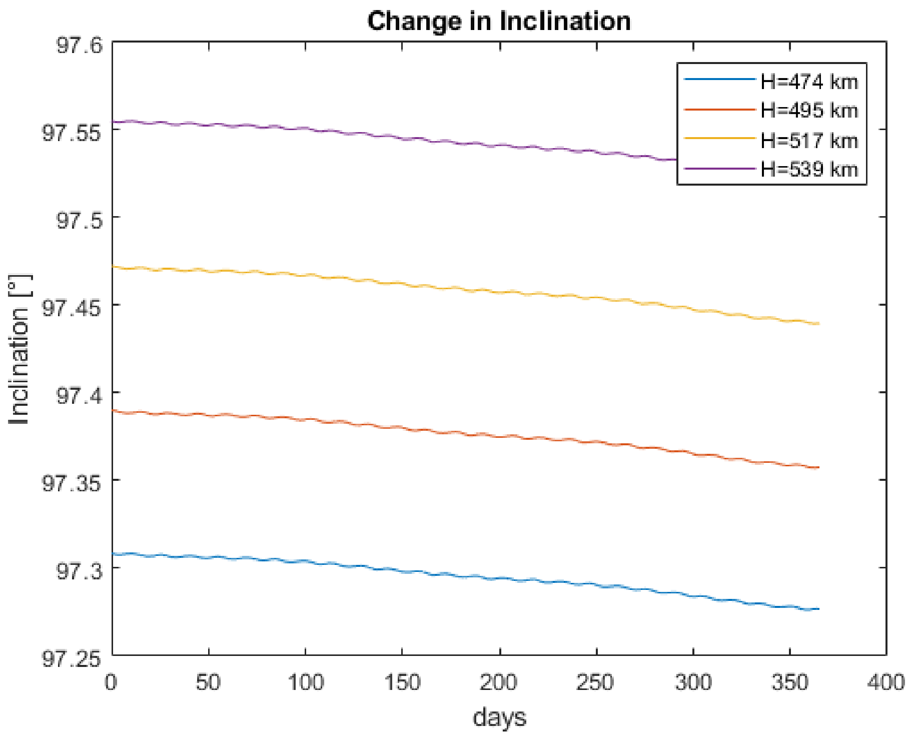

Figure 4.7: Orbital Parameter - Inclination

This estimate is also necessary for the subsequent sizing of the propellant tank, depending on the mass of propellant used, which can be easily obtained by multiplying the mass flow with the total transfer time, according to the relationship:

$$m_p = \dot{m} t_f \tag{4.9}$$

Solutions	Propellant Mass [kg]
1st - 474 km	0.81
2nd - 495 km	0.51
3rd - 517 km	0.35
4th - 535 km	0.33

Table 4.9: ΔV budget

The first mass estimate provides realistic data for all the proposed solutions, with values of less than 1 kg of propellant, which do not adversely affect the subsystem's sizing. Then, taking into account the coverage requirements, an assessment will be made for the final orbit to be selected.

Chapter 5

Communication Architecture

The purpose of this chapter is to evaluate as a function of access the amount of data that can be transferred in the S-band downlink for the payload and in both uplink and downlink in the UHF band for TT&C. This evaluation is supported by hyperspectral sensors, which, thanks to the high number of spectral bands, allow to identify differences between the samples analyzed.

In compliance with the mission requirements, different orbits will be analyzed to optimize the revisit time and evaluate the link availability with the ground stations that are part of the LeafSpace network, necessary for the link budget to transmit and receive information about payload and TT&C.

Taking into account the commercial off-the-shelf components available for the CubeSat, it has been possible to size a communication architecture based on the use of specific antennas and appropriate transceivers.

Finally, the link budget has been calculated to verify that there was a link channel between the satellite and the ground stations and that it could guarantee the correct transmission of the information at the expense of any losses.

5.1 Simulation Analysis

Entering into the details of the analysis, it was considered to monitor the area of Lake Como through the hyperspectral payload mounted on board with the following characteristics:

HyperSpectral Camera	
Sensor Detector	1000x1000 pixels
Spectral Range	450-950 nm
Spectral Resolution	8 nm
Spectral Bands	125
Bit Resolution	12 bit
FOV_{act}/FOV_{alt}	30°/16°

Table 5.1: Payload Characteristics

Through the use of the System Tool Kit (STK) software, for the orbits previously analyzed, a sensor was placed on the respective satellites with the Field of View seen in the table, so that the coverage in one year over the area of interest was evaluated, considering a sensor with push-broom scanning without moving parts pointing only to the nadir.

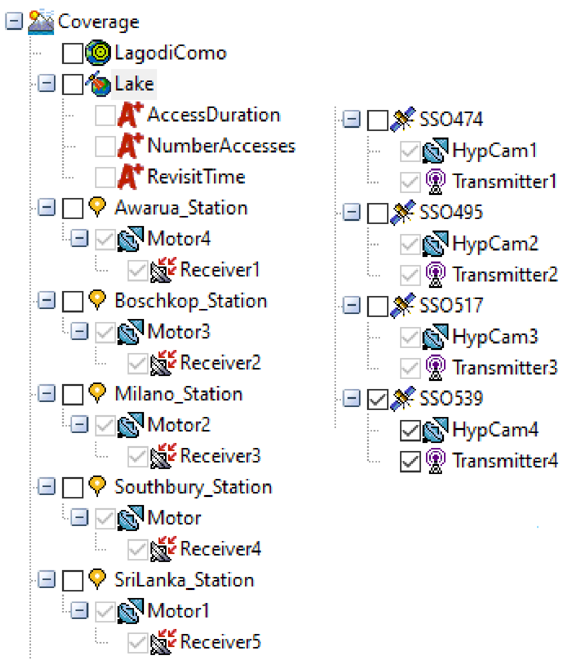

Figure 5.1: All Objects present in Simulation Environment STK

Three main satellite operational modes can be identified:

- *Acquisition mode*: The acquisition mode is in charge to acquire and keep a safe sun pointing attitude in order to guarantee the nominal platform performance. The attitude acquisition operations are performed autonomously on board, without intervention from ground, so that the satellite can survive waiting for commands from ground station. In acquisition mode the payload is switched off.

- Nominal mode: The nominal mode is dedicated to the payload operations. The DANTe-1 payload is in charge to acquire hyperspectral images of the Earth; therefore, the satellite attitude must be Nadir pointing during the images acquisition.

  However, the period required to acquire images is a small part of the overall mission, consequently it results convenient to keep a Sun pointing attitude when images are not acquired.Two main "sub-modes" of the Nominal mode can be identified:

  - Stand-by: During stand-by mode the satellite attitude control keeps the solar array pointed towards the Sun, while the payload is in stand-by waiting for the beginning of the images acquisition.

    This configuration maximizes the power S/S performance keeping as low as possible the overall power consumption, optimizing the power generated by the solar array and the battery charging.

  - Observation and download: The Observation and download mode have the purpose to acquire the hyperspectral images and to download them with in S band.

    Both download and observation must be performed with the satellite in Nadir pointing attitude, therefore an attitude manoeuvre will be executed prior and after observation and download operations.

- Safe mode: The satellite safe mode can be entered autonomously or by telecommand as a consequence of contingency situations. The transition to safe mode causes the payload switch off to safe power in order to guarantee as far as possible the satellite survival.

  The exit from Safe mode can be commanded only from ground after the execution of dedicated investigation and, if required, the implementation of the proper recovery actions.

To analyze Lake Como in STK, a coverage area was created with an extension that included its. A Coverage Definition is then inserted which, depending on the precision detail, provides for the definition of the point granularity of the grid.

In addition, to limit the computational cost, a value of 0.05 degrees was selected, which is equivalent to one grid point for every 30km^2. Figures of merit were then created to detail the analysis and assess the *number of accesses*, *duration*, and *revisit time*.

About the ground stations, those in Milan, Boschkop, Awarua, Southbury, and Sri Lanka have been chosen to guarantee almost global coverage, given their geographical layout.

Altitude[km]	N° of Accesses[1year]	Access Duration[s]	Revisit Time[d]
474.066	105	19.11	6.46
495.543	131	17.26	7.09
517.188	210	15.72	5.46
539.004	131	21.68	11.46

Table 5.2: Figures of Merit for Lake Como

Looking at the table, it can be seen that, although the duration of accesses has been reduced (the minimum duration of accesses has been taken into account in order to consider the worst case so that data can also be acquired in this condition) compared to the other solutions, the optimal altitude is 517 km, which offers advantages from the point of view of observation frequency, since the total number of annual accesses is almost double that of the other solutions, thanks also to a shorter revisit time.

A plan of observation campaigns shall be defined to test the functional operations of the Hyper-spectral imager. Command from ground will allows the payload to perform observations of an exact area in relation to an exact frequency of imaging. Collected information shall be analysed to verify the accuracy and the performances of the proposed observation techniques. Gathered data shall be shared into a cooperating ground stations network.

For the DANTe-1 mission it has been foreseen to use LeafLine he Ground Segment from LEAF SPACE. Leaf Line is a ground segment as-a-service which is tailored to the customer needs, including daily passes, pass distribution and operational conditions. The service is perfect for missions requiring high contact time and low latency, typical elements of Leaf Space distributed ground station network.

Using the Leaf Space API-rest (REpresentational State Transfer) it is possible to interact with the network, set the satellite parameters and constraints, retrieve the schedule of operations, and all the needed data. A real-time data exchange is guaranteed.

If needed Leaf Space can also provide LeafKey a custom and dedicated ground segment service. The Ground Stations of your Leaf Key network is specifically designed for the customer RF, baseband performance and security requirements. Leaf Space control all the supply and production chain to meet customer demands. The Ground Station locations are accurately selected taking into account customer mission or constellation orbits, contact time, latency, availability levels, security requirements and RF licensing.

In addition, similar characteristics have been assessed for the stations previously considered assigning a minimum elevation angle of $\varepsilon = 5$ deg to ensure correct communication, whose evaluation, however, will serve more for the calculation of the data rate necessary for the transfer of TT&C and payload data than as a discriminator between the different stations.

In this case, access times are of the order of minutes, bearing in mind that for ground communications, each ground station is equipped with a parabolic antenna which targets the satellite, thus increasing link availability, obtaining the following results:

Altitude[km]	N° of Accesses[1year]	Access Duration[s]	Revisit Time[h]
474.066	1617	414.79	5.30
495.543	1644	429.73	5.21
517.188	1670	445.31	5.12
539.004	1696	458.91	5.04

Table 5.3: Milano Station

Altitude[km]	N° of Accesses[1year]	Access Duration[s]	Revisit Time[h]
474.066	1460	424.51	5.88
495.543	1512	432.26	5.67
517.188	1512	452.72	5.66
539.004	1590	452.44	5.38

Table 5.4: Southbury Station

Altitude[km]	N° of Accesses[1year]	Access Duration[s]	Revisit Time[h]
474.066	1146	433.91	7.52
495.543	1199	439.25	7.18
517.188	1251	441.29	6.87
539.004	1303	447.7	6.59

Table 5.5: Boschkop Station

Altitude[km]	N° of Accesses[1year]	Access Duration[s]	Revisit Time[h]
474.066	1043	430.45	8.27
495.543	1096	433.08	7.87
517.188	1148	434.28	7.50
539.004	1148	455.98	7.49

Table 5.6: Sri Lanka Station

Altitude[km]	N° of Accesses[1year]	Access Duration[s]	Revisit Time[hr]
474.066	1668	413.52	5.13
495.543	1668	431.32	5.13
517.188	1668	452.98	5.12
539.004	1720	461.65	4.96

Table 5.7: Awarua Station

The stations examined represent a typical scheme of those that are feasible, with possible improvements in geographical location and number available. However, it is not necessary to guarantee complete daily time coverage, since in the situation analysed there is already an average of ≈22 daily passes.

They guarantee an almost real-time communication margin, every hour or so, sufficient for any communications and transmission of commands, as well as for the transmission of data on the payload, which do not have the same priority as TT&C data.

According to what has been observed in the previous chapter, given the savings from the ΔV point of view and for the orbital maintenance, which allows greater flexibility also for the sizing of the propulsion system, together with the higher frequency of observations that guarantees a higher quantity of scans compared to the other orbits with more constant monitoring due to the low revisit time, it is easy to suppose that the choice will fall on the orbit with altitude H=517 km, whose orbital parameters will be, therefore:

Parameters		
Orbital Height	h	517.188 km
Period	p	5690 s
Inclination	i	97.4718 °
Argument of perigee	ω	90°
Eccentricity	e	≈ 0
LTDN	-	10.30 a.m

Table 5.8: Orbital Parameters

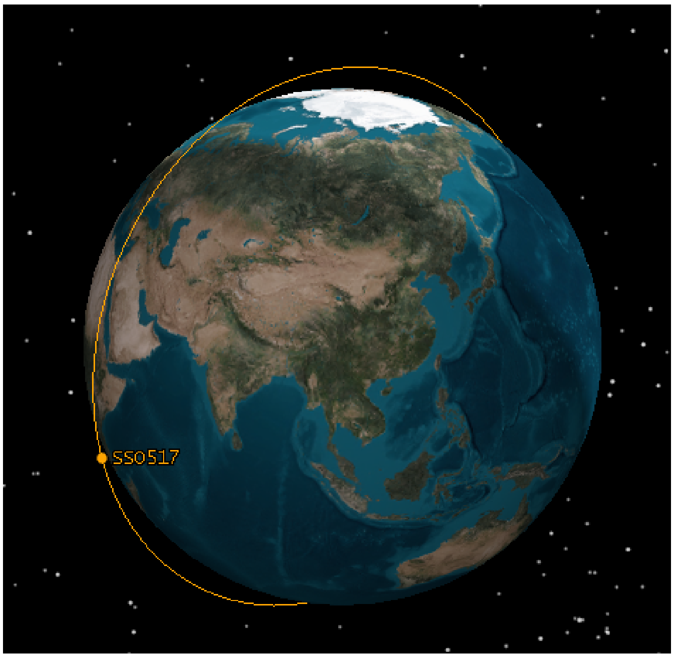

Figure 5.2: 3D Orbit from STK

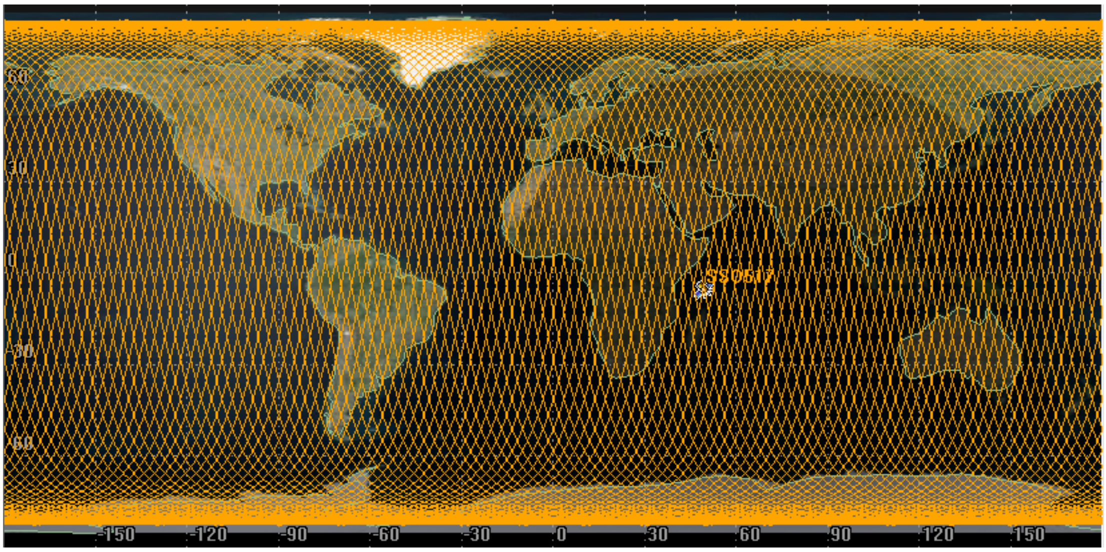

Figure 5.3: Ground Track after completed repeat cycle from STK

To generalize the previous analysis to demonstrate a global coverage of the satellite, one can analyze the ground track grid. Assume that the sensor has a wide swath width without tilt capability or the case where the sensor has tilt capability but a small swath width.

From the orbital data, the longitudinal separation S_t (westward) of the ground tracks, between successive passes at the equator measured at the ascending node, is given by:

$$S_Q = P(\omega_p - \dot{\Omega}) \tag{5.1}$$

where ω_p is the angular velocity of the planet about the polar axis and $\dot{\Omega}$ is the rate of change of line of nodes. From here, introducing the parameter Q indicating the number of daily orbits, the longitudinal separation can also be written:

$$S_Q = \frac{2\pi}{Q} = 23.778° \approx 2646.9km \tag{5.2}$$

At the end of the repeat cycle, it is possible to identify the minimum interval on the equator between two tracks on the ground:

$$S_N = \frac{S_Q}{N} = 1.698° \approx 189.06km \tag{5.3}$$

To verify that the satellite covers the entire surface of the earth, one can relate the calculated swath width at the equator to the minimum interval. If the latter is greater, it can be said with certainty that there are no gaps in coverage.

To obtain a more accurate result, the apparent inclination i' is introduced. The apparent inclination is the angle between the equator and the ground track of the satellite in an Earth-centered coordinate system (ECEF) and is defined as:

$$\tan i' = \frac{\sin i}{\cos i - 1/Q} \tag{5.4}$$

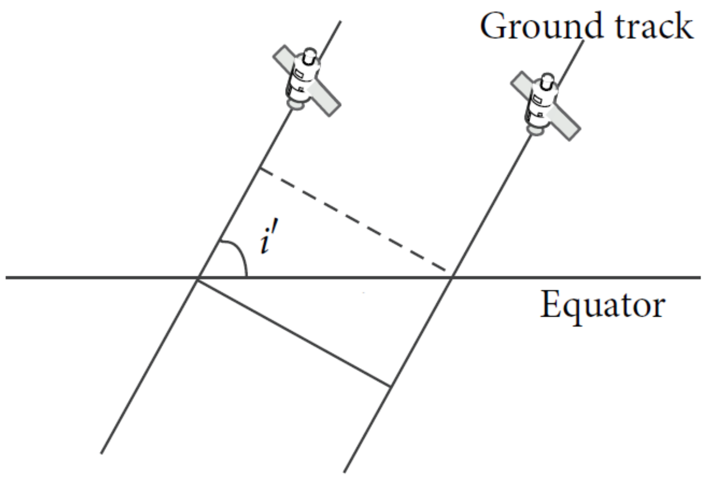

Figure 5.4: Apparent inclination on the equator.

Calculating the swath width at the equator using the formula:

$$Sw'_{act} = \frac{Sw_{act}}{\sin i'} \approx 282.82km \tag{5.5}$$

It can be verified how even considering a safety margin for a required overlap of 10% (replacing the width of the actual swath with $0.9Sw_{act}$):

$$Sw'_{act} > S_N$$

so the satellite in adjacent orbits can observe the ground target, thus making the revisit time less than the repeat cycle and this provides a total coverage demonstrating how it is possible to make through these observations in every part of the globe. [19]

5.2 Data Rate

At this point it is possible to determine the amount of data produced by the payload and TT&C to then correctly size the on-board systems for data transmission to the ground stations.

The architecture of the satellite is of the store-and-forward type. In this configuration, the satellite will make a low orbit trajectory and, when it comes in sight of the ground station, will transmit the data collected in previous orbits, stored in a memory.

The main advantages of this architecture are the low cost of the satellite and of putting it into orbit, the possibility of installing a low-directivity antenna, which makes it possible to reduce its size and allows greater tolerance for its pointing.

5.2.1 Payload

Since the satellite mounts a hyperspectral sensor with a push-broom scanner, it is possible to assume that the instantaneous field of view coincides with the field of view, since it can scan a complete row of n cells as it passes over the area to be observed. Depending on the performance of the hyperspectral camera, we first evaluate the volume of data generated by a single shot, starting with the calculation of the observable area at nadir:

$$Sw_{act} = 2H\tan\left(\frac{FOV_{act}}{2}\right) = 277.16km \tag{5.6}$$

$$Sw_{alt} = 2H\tan\left(\frac{FOV_{alt}}{2}\right) = 145.37km \tag{5.7}$$

$$A = Sw_{act} \cdot Sw_{alt} = 36989.43km^2 \tag{5.8}$$

From the number of spectral bands (N_b) and the camera resolution (P_r), knowing that each pixel is encoded by 14 bits, the data volume associated with one image is:

$$V = P_r \cdot N_b \cdot B = 1500Mbit \tag{5.9}$$

Since the average revisit time for Lake Como is about $\approx$ 5.46 days, it can be assumed, knowing the track of the satellite, that the nominal observation phase is activated only during the passage over it, thus avoiding overloading the OBC memory with useless data. To calculate the data rate it is necessary to divide the amount of data generated (to be transferred) by the access time with the ground stations:

$$DR = \frac{V}{t_a} \tag{5.10}$$

In this scenario have been considered the case where the area is only scanned once for each pass evaluating the data rate associated with the transmission of such data and then checking the link budget.

From the above data, it can be seen that the satellite connects with the ground stations about four times a day. Starting from this consideration, it is possible to divide up the transfer of payload data (with a lower priority than telemetry data) for the aforementioned accesses, in order to transfer them completely in a single day, obtaining for different stations:

Ground Stations	Data Rate [Mbit/s]
Milano	0.84
Southbury	0.83
Boschkop	0.85
Awarua	0.82
Sri Lanka	0.86

Table 5.9: Data Rate in one day for each Station - 1 Image

To fulfil this task, the following components, whose characteristics are given in the appendix, have been selected from Isispace, that provides turn-key CubeSat and nanosat solutions for both governmental and commercial customers around the globe, working with a broad range of standardized CubeSat parts and if needed, customized solutions:

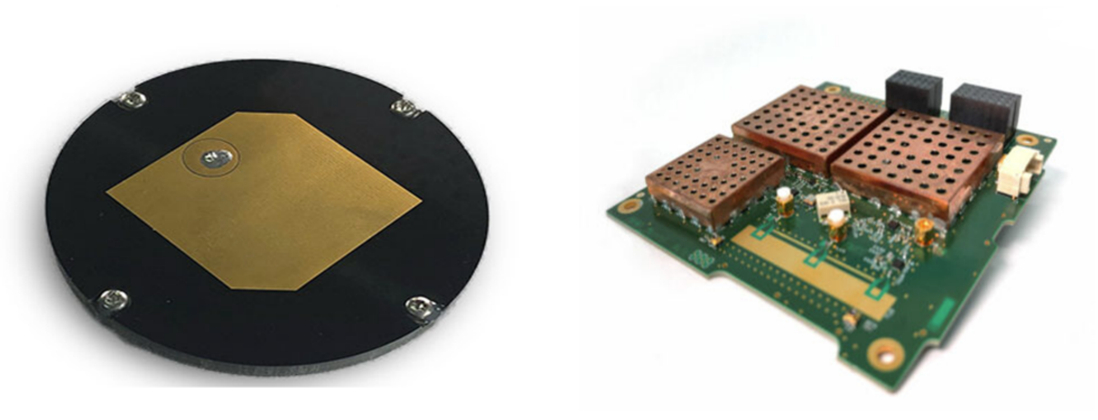

Figure 5.5: S-band Patch Antenna (left) and S-band Transceiver (right) from Isispace

Thanks to the transmitter's data transfer capacity of up to 10Mbit/s, it can be assumed that many more measurements can be made during a single pass. In this respect, based on a precautionary margin due to connection delays, a total number of 10 scans per pass was assumed.

In this way, however, despite the availability of transferring data at a specific data rate, problems occurred during the link budget, which returned negative values, confirming the difficulty of establishing a stable connection.

By trial and error, the maximum number of scans (seven per pass) was determined, allowing a good margin to ensure correct communication at the expense of possible losses, by returning the following data rates:

Ground Stations	Data Rate [Mbit/s]
Milano	5.89
Southbury	5.80
Boschkop	5.94
Awarua	5.79
Sri Lanka	6.04

Table 5.10: Data Rate in one day for each Station - 7 Images

5.2.2 Tracking, Telemetry & Command

A different situation applies to this type of data. First of all, these data are collected by the satellite to monitor the activities of the subsystems associated with it, or in general, they can be associated with commands that are transmitted by the ground stations, such as requests for data transmission or attitude corrections to ensure correct pointing at any given moment.

To guarantee a good data rate in the UHF band and a correct match for the frequencies between the transmitting and receiving antenna (as was also done in the case of the S-band payload data), the following components have been selected:

For this analysis, therefore, reference was made to the transceiver's ability to transmit data at a maximum speed of 19.2 kbit/s with moderate power usage. Initially, the idea was to take measurements every second to monitor the satellite and associated subsystems as constantly as possible and then evaluate the difference between the data generated and the data that can be transferred, to see if it is possible to increase or decrease the frequency with which they are collected.

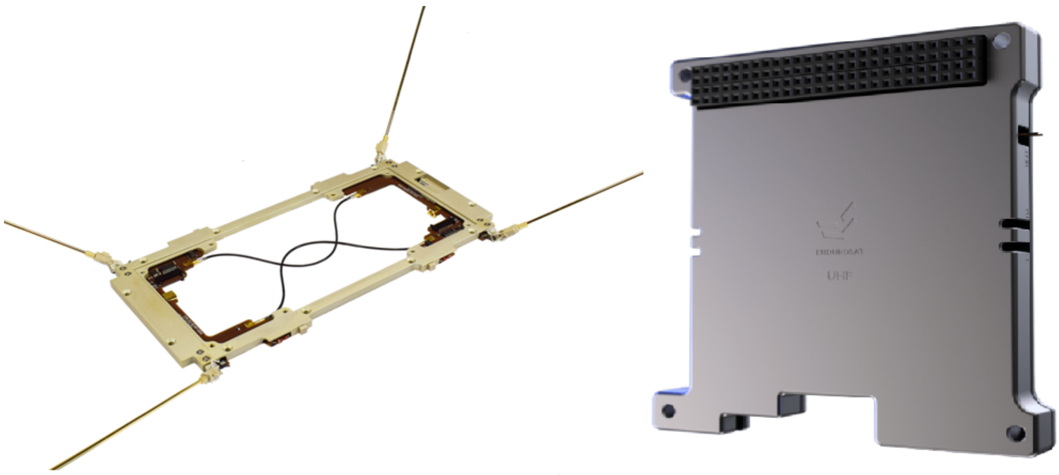

Figure 5.6: UHF Deployable Antenna (left) and UHF-band Transceiver (right) from Isispace and Endurosat

At this stage, since no detailed architecture of the subsystems has been specified, it is possible to make an initial estimate of the signals collected, which can then be further optimised in the subsequent phases of the mission.

Assuming that each signal is collected as a 4-byte (32-bit) data item, it is possible to classify signals collected through macro-categories, obtaining:

Subsystem	N° of measures	bit/s
Payload	3	96
Power	17	544
Propulsion	8	256
AODCS	31	932
Mechanisms	5	192

Table 5.11: Signals collected by satellite - First try

Assuming an average of 4 accesses per day for each station, it can be assumed a passage every 6 hours during which the satellite makes approximately ≈3.8 orbits. Taking into account the signals considered in the table above, we can calculate the number of data generated in one orbit and subsequently:

$$D_g = 3.8 \cdot 11493.95 = 43632\ kbit = 43.632\ Mbit \tag{5.11}$$

Given the duration of each access to the station and the maximum data rate guaranteed by the transmitter, it is easy to calculate the amount of data that can be transferred during one pass (The Milan station has been taken as an example, but a similar procedure holds true for other stations):

$$D_t = 19.2 \cdot 445.307 = 8459.89\ kbit = 8.55\ Mbit \tag{5.12}$$

It is immediately evident that the amount of data cannot be transferred in the estimated time:

$$\Delta D = D_t - D_g = -35.08\ Mbit \tag{5.13}$$

It can be seen that the balance is negative and therefore the volume produced between consecutive passes exceeds the amount of data that can be transferred. At this point, it is clear that it is necessary to reduce the amount of data produced by the instrumentation.

Possible values have been found by iterating, however, differentiating the frequency of data collection for the different subsystems. In particular, higher priority has been given to data collected from the payload and the power system. The new values are listed in the following table:

Subsystem	N° of measures	bit/s
Payload	3	96
Power	17	108.8
Propulsion	8	25.6
AODCS	31	93.2
Mechanisms	5	19.2

Table 5.12: Signals collected by satellite - Possible solution

Proceeding in the same way as in the previous case, the following difference is obtained:

$$\Delta D = D_g - D_t = 1.15\ Mbit \tag{5.14}$$

Keep in mind that this solution is not the optimal one, but it guarantees the transfer of all data in the time needed, with a good margin.In this respect, the solution analysed makes it possible not to produce more data than could be transmitted and to leave sufficient room in the available time window for supplementary and service communications.

This choice has been preferred in this case, as the idea of ensuring that the data collected between two consecutive passes is always fully transferable makes it easier to design the satellite control system, at the expense of a more optimised number of measurements taken.

Appropriate changes can be considered depending on mission requirements, by giving priority to specific subsystems or increasing the number of stations in the network to combining them and increase access times, to decrease the data rate.

5.3 Link Design

As mentioned in the previous paragraphs, the DANT-e satellite mounts two transmitters as it has to operate in different bands. Therefore, it will be necessary to consider that a specific budget link for the payload communication channel operating in S-band and a specific one for TT&C data transmission operating in the UHF band.

For the former, only the evaluation of the downlink phase will be required, since DANT-e can only transmit the data it collects and cannot communicate with other satellite constellations in orbit, while for telemetry communications it is necessary to verify that a communication channel is established for both downlink and uplink, taking into account any requests that ground antennas may send to it.

5.3.1 Coding and Modulation

Before determining the basic parameters of link design, it is necessary to introduce the concept of modulation, i.e. the technique whereby the signal to be transmitted is generally associated with a carrier wave in order to better adapt it to transmission.

In general, depending on the parameters that are modified in the modulated wave, we speak of modulation in amplitude, frequency, or phase. In our case, since it is possible to configure the modulation of the ground stations, this will be dictated solely by the satellite transceivers.

We will see specifically for S-band the Binary phase-shift keying (BPSK) that consists of setting the carrier phase at 0 deg to transmit a binary 0, and setting the phase at 180 deg to transmit a binary 1. Instead, for UHF band Frequency shift keying (FSK) that sets the carrier frequency at F1 to transmit a binary 0, and at F2 to transmit a binary 1 [17].

The multiple frequency shift keying (MFSK) is similar to frequency shift keying (FSK) with the exception that more than two frequencies are employed, as shown in the following figure:

Demodulation of the signal at the receiver consists of measuring the variations in the characteristics of the received carrier and deducing what the original signal was. FSK and MFSK modulated signals are usually demodulated by measuring the received power at each of the possible frequencies, and selecting the frequency with the highest power as the transmitted one. An advantage of this technique is that

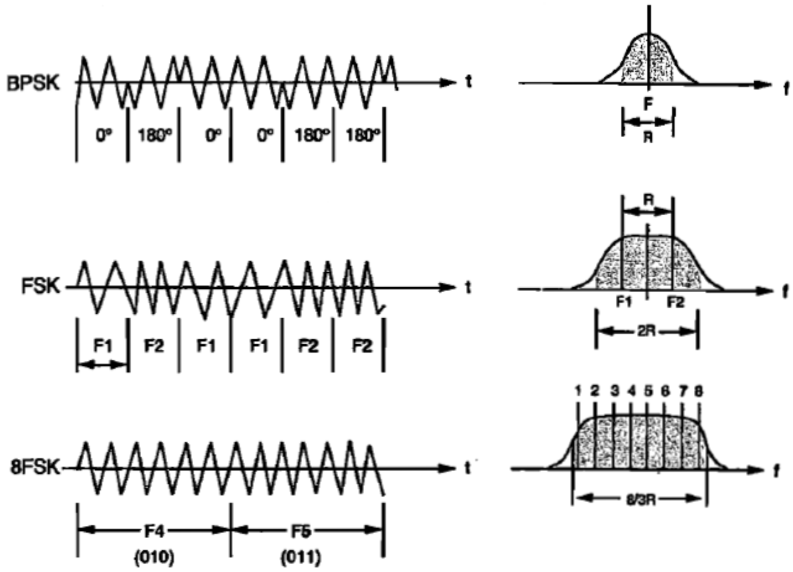

Figure 5.7: Modulation Types Commonly Used in Satellite Communications

any change in the phase of the carrier introduced by the transmission channel will not greatly degrade the performance of the link. For this reason, these modulations are often used in command links (FSK modulation of a sub-carrier).

On the other hand, BPSK demodulation requires the phase of the received carrier to be measured, but suffers from the phase distortion caused by the transmission channel, which significantly degrades performance [17].

5.3.2 Link Budget

Link budget relates the transmit power and the receive power and shows in detail how the difference between these two is accounted for, as well as the overall customer satisfaction with the satellite service.

To this end the fundamental elements of the communications satellite Radio Frequency (RF) or free space link are employed. It is a tabular method for evaluating the power received and the noise ratio in a radio link and is usually calculated for a worst-case scenario, the one in which the link will have the lowest C/N ratio or lowest tolerable availability.

In this case it is possible to consider a minimum elevation angle equal to $\varepsilon = 5$ deg, which at the same time generates high values of atmospheric attenuation and thus has a significant influence on the total margin, which will therefore be very constrained, in contrast to increasing elevation angle values which result in better attenuation and an increasing margin.

The above relationships are made explicit in the following expression, which is generally used to size a digital data link:

$$\frac{E_b}{N_0} = \frac{PL_lG_tL_sL_aG_r}{kT_sR} \tag{5.15}$$

in which therefore appear the power associated with the transmitter (P), the two antenna gains (transmitter G_t and receiver G_r), the data rate (R), and the various associated losses such as those between transmitter and antenna (L_l), or those of free space losses (L_s) or even propagation path length (L_a), as well as Boltzmann's constant (k) and the noise temperature of the system (T_s).

The link equation is a product of successive terms and, therefore, can be conveniently expressed in terms of decibels or dB. A number expressed in dB is just 10 log_{10} of the number. The equation can be rewritten as follows:

$$\frac{E_b}{N_0} = P + L_t + G_t + L_{\theta r} + L_s + L_a + G_r + 228.6 - 10log(T_s) - 10log(R) \tag{5.16}$$

Or, to compact the first three terms, it is possible to introduce Effective Isotropic Radiated Power (EIRP) and write:

$$\frac{E_b}{N_0} = EIRP + L_{\theta r} + L_s + L_a + G_r + 228.6 - 10log(T_s) - 10log(R) \tag{5.17}$$

Before proceeding to calculate the link budget according to the parameters also associated with the subsystems chosen in the previous steps, it is good to have a conceptual discussion about the losses and noise temperature of the system, negatively affecting the margin.

5.3.3 Losses and System Noise Temperature

In sequential order, the first losses to be addressed are those between the transmitter and the antenna L_l, which are highly dependent on the presence of any filter stage or diplexer, generally used to share a communication channel, as well as the presence of coaxial cables used to connect the devices, whose losses should be quantified according to their length. All these elements cause a signal attenuation that is typically between 1dB and 3dB.

It is also possible to classify the losses due to space L_s, which have the greatest impact on the overall balance, since the power density transmitted by the antenna, as the distance at which the signal is received increases, is distributed, more or less uniformly, over an increasingly greater area, which increases with the square of the distance.

The contact with the ground station occurs when the satellite rises above the station's horizon and lasts until, as it travels along its orbit, it sets below the same horizon line. The distance will be equal to the altitude of the orbit only when the satellite will pass the zenith of the ground station, in all other cases the distance will be greater.

Given the slant range (D) between the transmitting and receiving station:

$$D = R_e \left[\sqrt{\left(\frac{R_e + H}{R_e} \right)^2 - \cos\varepsilon^2} - \sin\varepsilon \right] \tag{5.18}$$

and transmission frequency (f) the attenuation of free space expressed in dB is given by the following relationship:

$$L_s = 20log(3 \cdot 10^8) - 20log(4\pi) - 20log(D) - 20log(f) \tag{5.19}$$

Within the distance, the minimum elevation angle also appears, which, as mentioned above, increases the value of losses, as can also be seen from the following [fig. 5.8] for downlink payload data, but a similar reasoning can be applied to other transmissions as well:

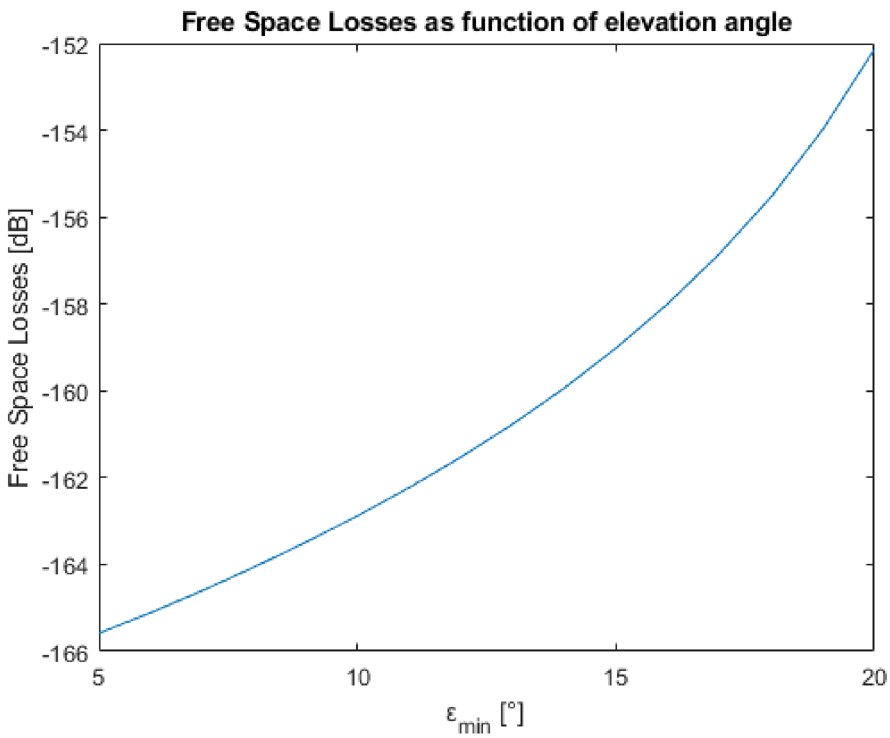

Figure 5.8: Free Losses as function of minimum elevation angle

Then, there are the losses associated with error pointing of the antenna L_p, which may not be located in the center of the transmitter antenna beam, or vice versa.

This can be caused by satellite stabilization problems or climatic factors, significantly decreasing the gain, which can be estimated once the pointing offset from the center of the beam (e) and the beamwidth of the transmitting antenna (θ) are known:

$$L_\theta = -12\left(\frac{e}{\theta}\right)^2 \tag{5.20}$$

Finally, not to be overlooked, are the propagation losses that contribute to the margin reduction. These include all effects due to polarisation mismatch, atmospheric gases, and ionosphere, as well as attenuation due to rain, which can be obtained from special tables. Typically, random losses in the order of 1dB are also added.

The system noise temperature is the sum of several individual contributions from various sources, depending on whether they are generated between the antenna terminal and the receiver output, depending on the transmission lines and filters and low noise amplifiers or otherwise generated by external factors, objects in the vicinity of the station, etc. In conclusion, the noise temperature of the system is given by:

$$T_s = T_{ant} + \left(\frac{T_0(1 - L_r)}{L_r}\right) + \left(\frac{T_0(F - 1)}{L_r}\right) \tag{5.21}$$

where F indicate the noise figure of receiver, the first term represents the noise antenna temperature, the second term is the noise contribution from the transmission line and the last is the contribution from the receiver.

5.3.4 Downlink - Payload

A careful choice of components has made it possible to operate in the same frequency spectrum. Then, it has been selected 2200 Mhz frequency, for which authorization from the Federal Communications Commission (FCC) will then be requested. Considering that for this purpose, a patch antenna is mounted on the satellite with fixed characteristics, as well as those of the parabolic antenna offered by LeafSpace for the ground station, with known features, it has been possible to obtain the following data:

Item	Symbol	Units	Values
Transmitter Power	P	Watts	13
Transmitter Power	P	dBW	11.14
Transmitter Line Loss	L_l	dB	-0.5
Peak Transmit Antenna Gain	G_{pt}	dB	6.5
Transmit Antenna Beamwidth	θ_t	deg	100
Transmit Antenna Pointing Offset	e_t	deg	10
Transmit Antenna Pointing Loss	L_{pt}	dB	-0.12
Transmit Antenna Gain (net)	G_t	dB	6.38
Equiv. Isotropic Radiated Power	EIRP	dBW	17.02
Space Loss	L_s	dB	-165.59
Atmospheric Loss	L_a	dB	-4.50
Peak Receive Antenna Gain	G_{rp}	dB	34.9
Receive Antenna Beamwidth	θ_r	deg	3
Receive Antenna Pointing Error	e_r	deg	0.3
Receive Antenna Pointing Loss	L_{pr}	dB	-0.12
Receive Antenna Gain (net)	G_r	dB	34.78
System Noise Temperature	T_s	K	431
Data Rate	R	bit/s	$5.8 \cdot 10^6$
E_b/N_0	E_b/N_0	dB	16.14

Table 5.13: Link Budget for Downlink - S band

It is possible to establish a relationship between the bit error rate and the margin required by the system, as shown in the following figure: Having set the former

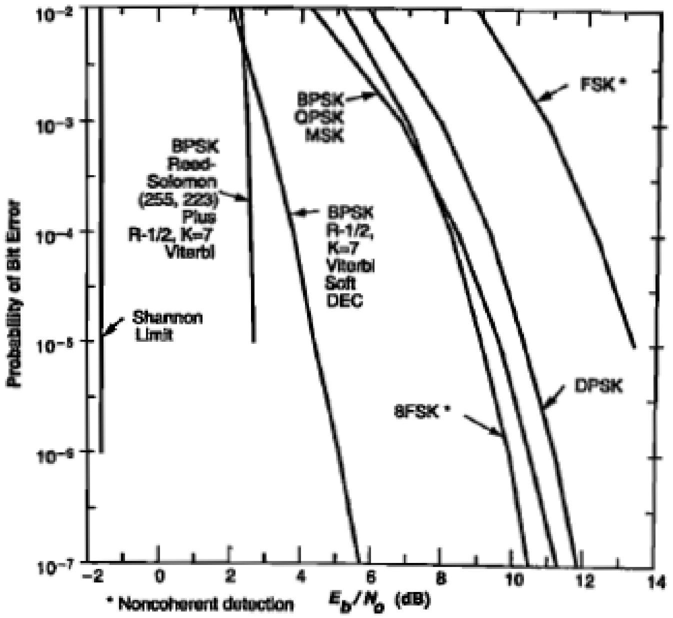

Figure 5.9: Bit error rate as a function of E_b/N_0

around a value of $BER = 10^-5$ and the type of modulation used (BPSK), it can be obtained the value of $E_b/N_0 \approx 9.6$. In addition, to establish a connection, it will be necessary to verify that the difference between the calculated margin and the required margin is greater than 3dB, which is fulfilled in this case:

$$Link\ Margin = \left(\frac{E_b}{N_0}\right) - \left(\frac{E_b}{N_0}\right)_{req} = 4.84dB \tag{5.22}$$

One could plot the various margin values obtained at different elevation angles, but from the [fig.5.8] it can be seen that it increases for increasing values of ε, so it was simply a matter of checking that there is a worst-case connection ($\varepsilon = 5$deg).

5.3.5 Downlink and Uplink - TT&C

In the case of TTC, also depending on the components chosen, the frequency band in which we operate in UHF, with a chosen frequency of 401 Mhz and supporting a 4FSK modulation.

In this case, since there is an exchange of information between the satellite and the ground station, it will also be necessary to consider the uplink. Unlike the parabolic antenna used for the S-band, in this case, the ground station mounts a set of 32-element Yagi-Uda antennas whose specifications are given in the table:

Item	Symbol	Units	Values
Transmitter Power	P	Watts	2
Transmitter Power	P	dBW	3.01
Transmitter Line Loss	L_l	dB	-0.5
Peak Transmit Antenna Gain	G_{pt}	dB	3
Transmit Antenna Beamwidth	θ_t	deg	94.87
Transmit Antenna Pointing Offset	e_t	deg	9.49
Transmit Antenna Pointing Loss	L_{pt}	dB	-0.12
Transmit Antenna Gain (net)	G_t	dB	2.88
Equiv. Isotropic Radiated Power	EIRP	dBW	5.39
Space Loss	L_s	dB	-150.8
Atmospheric Loss	L_a	dB	-3.80
Peak Receive Antenna Gain	G_{rp}	dB	14.8
Receive Antenna Beamwidth	θ_r	deg	27
Receive Antenna Pointing Error	e_r	deg	2.70
Receive Antenna Pointing Loss	L_{pr}	dB	-0.12
Receive Antenna Gain (net)	G_r	dB	14.68
System Noise Temperature	T_s	K	895
Data Rate	R	bit/s	$1.9 \cdot 10^4$
E_b/N_0	E_b/N_0	dB	20.35

Table 5.14: Link Budget for Downlink - UHF band

It is possible to repeat the previous process to evaluate the margin required by the system and finally calculate the difference to guarantee the linking balance, which is also satisfied in this case:

$$\textit{Link Margin} = \left(\frac{E_b}{N_0}\right) - \left(\frac{E_b}{N_0}\right)_{req} = 10.35dB \tag{5.23}$$

Finally, for the uplink, for which, among other things, we try to minimize errors as much as possible, further reducing the bit error rate $\approx 10^{-7}$, the result is: Finally,

Item	Symbol	Units	Values
Transmitter Power	P	Watts	100
Transmitter Power	P	dBW	20
Transmitter Line Loss	L_l	dB	-0.5
Peak Transmit Antenna Gain	G_{pt}	dB	14.80
Transmit Antenna Beamwidth	θ_t	deg	27
Transmit Antenna Pointing Offset	e_t	deg	2.70
Transmit Antenna Pointing Loss	L_{pt}	dB	-0.12
Transmit Antenna Gain (net)	G_t	dB	14.68
Equiv. Isotropic Radiated Power	EIRP	dBW	34.18
Space Loss	L_s	dB	-151.26
Atmospheric Loss	L_a	dB	-3.80
Peak Receive Antenna Gain	G_{rp}	dB	3
Receive Antenna Beamwidth	θ_r	deg	94.87
Receive Antenna Pointing Error	e_r	deg	9.49
Receive Antenna Pointing Loss	L_{pr}	dB	-0.12
Receive Antenna Gain (net)	G_r	dB	2.88
System Noise Temperature	T_s	K	1185
Data Rate	R	bit/s	$1.9{\cdot}10^4$
E_b/N_0	E_b/N_0	dB	36.90

Table 5.15: Link Budget for Uplink - UHF band

the difference between the margins will be equal in this case to:

$$Link\ Margin = \left(\frac{E_b}{N_0}\right) - \left(\frac{E_b}{N_0}\right)_{req} = 24.90dB \tag{5.24}$$

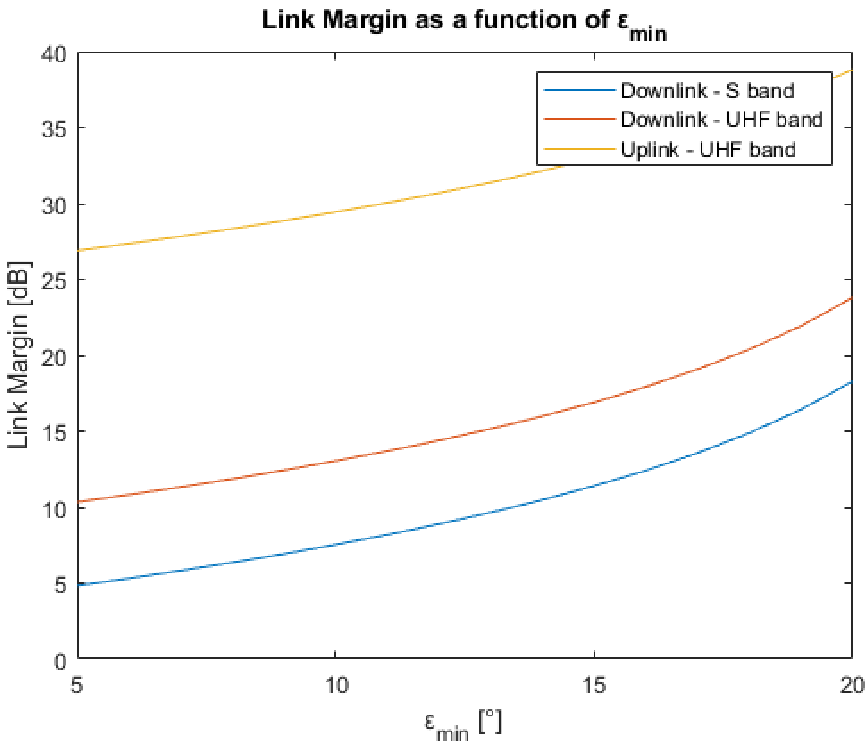

Figure 5.10: Link Margin as a function of minimum elevation angle

The dependence of the link budget on the minimum elevation angle is important and should be chosen wisely, depending on the area in which the ground stations are located. In our case, however, since we could refer to many more stations, thanks to the geographical distribution of the network made available, we preferred to evaluate the worst case to guarantee correct communication and avoid problems.

Chapter 6

Conclusions

The preliminary analysis confirms first of all the importance of the choice of the orbit that guarantees a total coverage leaving ample possibilities of observation for the different terrestrial zones, as well as a low cost in terms of ΔV and therefore for the orbital maintenance.

Entering into detail, the frequency of observation of the area of interest was taken into account and it was seen how the latter was optimized with the support of simulations carried out in STK, thus allowing to minimize the revisit time, less than the repeat cycle and reduced to a few days, ensuring constant monitoring through hyperspectral observations, thus ensuring the feasibility of the mission.

A further improvement could be made by realizing a Walker constellation with two or more DANT-e satellites staggered on the same orbital plane, with the possibility to communicate with each other and better manage the data transferable to ground stations at any time, taking advantage of piggyback launches without excessive additional costs.

Or again, it could be considered to implement an attitude control algorithm that, if envisioned in the design phase, would greatly increase access times for both stations and the area of interest,in parallel with a different geographical dislocation of the ground stations made available by the LeafSpace network, which would be instrumental in significantly reducing the data rate, perhaps allowing for the rework of the COTS components used to further minimize the power required for nominal operations.

Bibliography

[1] J Foley. «The CubeSat Program». In: *California Polytechnic Institute, San Luis Obispo* (1999) (cit. on p. 1).

[2] «CubeSat Market Projection according to Allied Market Research». In: (). URL: https://www.prnewswire.com/news-releases/cubesat-market-to-reach-491-3-mn-globally-by-2027-at-15-1-cagr-allied-market-research-301220994.html (cit. on p. 2).

[3] «Launched, planned and predicted CubeSats as of January 2020». In: (). URL: https://www.nanosats.eu/ (cit. on p. 2).

[4] «Remote Sensing». In: (). URL: https://www.omnisci.com/technical-glossary/remote-sensing (cit. on p. 3).

[5] «Storia del telerilevamento». In: (). URL: https://www.planetek.it/formazione/manuali_on_line/corso_di_telerilevamento_on_line/2_breve_storia_del_telerilevamento (cit. on p. 3).

[6] «Dem Spatial Resolution – What Does This Mean». In: (). URL: https://www.jbarisk.com/news-blogs/dem-spatial-resolution-what-does-this-mean-for-flood-modellers/ (cit. on p. 4).

[7] Michael R Heffels and Joaquin Vanschoren. «Aerial Imagery Pixel-level Segmentation». In: *arXiv preprint arXiv:2012.02024* (2020) (cit. on p. 5).

[8] M Govender, K Chetty, V Naiken, and H Bulcock. «A comparison of satellite hyperspectral and multispectral remote sensing imagery for improved classification and mapping of vegetation». In: *Water SA* 34.2 (2008), pp. 147–154 (cit. on p. 6).

[9] «Hyperspectral and Multispectral Imaging». In: (). URL: https://www.edmundoptics.com/knowledge-center/application-notes/imaging/hyperspectral-and-multispectral-imaging/ (cit. on pp. 7, 8).

[10] Telmo Adão, Jonáš Hruška, Luís Pádua, José Bessa, Emanuel Peres, Raul Morais, and Joaquim Joao Sousa. «Hyperspectral imaging: A review on UAV-based sensors, data processing and applications for agriculture and forestry». In: *Remote Sensing* 9.11 (2017), p. 1110 (cit. on p. 8).

[11] Alessandro A Quarta and Giovanni Mengali. «Fondamenti di meccanica del volo spaziale». In: *Fondamenti di meccanica del volo spaziale* (2013), pp. 1–788 (cit. on pp. 10, 11).

[12] Craig A Kluever. *Space flight dynamics*. John Wiley & Sons, 2018 (cit. on p. 18).

[13] Roger R Bate, Donald D Mueller, Jerry E White, and William W Saylor. *Fundamentals of astrodynamics*. Courier Dover Publications, 2020 (cit. on p. 18).

[14] Hanneke de Jong. «Analytical Low-Thrust Trajectory Design: Using the Simplified General Perturbations Model». In: (2018) (cit. on p. 23).

[15] Jindong Li. «Satellite Remote Sensing Tecnhology». In: () (cit. on p. 30).

[16] G Lucarelli-S Troisi. «Problemi di Navigazione Spaziale». In: () (cit. on p. 30).

[17] Wiley J Larson and James Richard Wertz. *Space mission analysis and design*. Tech. rep. Torrance, CA (United States); Microcosm, Inc., 1992 (cit. on pp. 36, 56, 57).

[18] ESA Unclassified – For Official Use. «Margin philosophy for science assessment studies». In: (2012) (cit. on p. 39).

[19] Xin Luo, Maocai Wang, Guangming Dai, and Xiaoyu Chen. «A novel technique to compute the revisit time of satellites and its application in remote sensing satellite optimization design». In: *International Journal of Aerospace Engineering* 2017 (2017) (cit. on p. 50).